1974-06

Breakdown phenomena in rare and in molecular gases using pulsed carbon dioxide laser radiation

Behrens, Peter

Monterey, California. Naval Postgraduate School

BREAKDOWN PHENOMENA IN RARE AND IN MOLECULAR GASES USING PULSED CARBON DIOXIDE LASER RADIATION

Peter Behrens

NAVAL POSTGRADUATE SCHOOL
Monterey, California

THESIS

BREAKDOWN PHENOMENA IN RARE AND IN MOLECULAR GASES USING PULSED CARBON DIOXIDE LASER RADIATION

by

Peter Behrens

June 1974

Thesis Advisor A.W. Cooper

UNCLASSIFIED

SECURITY CLASSIFICATION OF THIS PAGE (When Data Entered)

REPORT DOCUMENTATION PAGE		READ INSTRUCTIONS BEFORE COMPLETING FORM
1. REPORT NUMBER	2. GOVT ACCESSION NO.	3. RECIPIENT'S CATALOG NUMBER
4. TITLE (and Subtitle) Breakdown Phenomena in Rare and in Molecular Gases Using Pulsed Carbon Dioxide Laser Radiation		5. TYPE OF REPORT & PERIOD COVERED Master's Thesis; June 1974 6. PERFORMING ORG. REPORT NUMBER
7. AUTHOR(s) Peter Behrens		8. CONTRACT OR GRANT NUMBER(s)
9. PERFORMING ORGANIZATION NAME AND ADDRESS Naval Postgraduate School Monterey, California 93940		10. PROGRAM ELEMENT, PROJECT, TASK AREA & WORK UNIT NUMBERS
11. CONTROLLING OFFICE NAME AND ADDRESS Naval Postgraduate School Monterey, California 93940		12. REPORT DATE June 1974 13. NUMBER OF PAGES 89
14. MONITORING AGENCY NAME & ADDRESS(if different from Controlling Office) Naval Postgraduate School Monterey, California 93940		15. SECURITY CLASS. (of this report) Unclassified 15a. DECLASSIFICATION/DOWNGRADING SCHEDULE

16. DISTRIBUTION STATEMENT (of this Report)

Approved for public release; distribution unlimited.

17. DISTRIBUTION STATEMENT (of the abstract entered in Block 20, if different from Report)

18. SUPPLEMENTARY NOTES

19. KEY WORDS (Continue on reverse side if necessary and identify by block number)

Gas Breakdown
CO_2 TEA Laser
Self-Focusing
Laser Spark Production

20. ABSTRACT (Continue on reverse side if necessary and identify by block number)

Light from an atmospheric pressure, double-discharge CO_2 laser was focused in monatomic and in diatomic gases at pressures from 0.01 atm to 10 atm in order to produce optical breakdown. The gases under investigation were Ar, He, N_2, H_2, and air. Measurements of the transmitted laser intensity were obtained and the properties of the resulting spark were studied by means of an open face camera and spectroscopic

DD FORM 1 JAN 73 1473 (Page 1) EDITION OF 1 NOV 65 IS OBSOLETE S/N 0102-014-6601 1

UNCLASSIFIED

SECURITY CLASSIFICATION OF THIS PAGE (When Data Entered)

(20. ABSTRACT continued)

techniques. For all gases studied the threshold power density was on the order of tens of gigawatts per square centimeter and decreased with increasing focal volume or gas pressure. The theoretical model was based on classical microwave cascade theory. The importance of loss terms other than electron diffusion loss was discussed. In the presence of preionization the threshold was on the order of hundreds of megawatts per square centimeter and showed no volume dependence. Emission spectra consisted of a strong continuum superimposed with strong lines due to neutral and ionized atoms. Results of this study were in good agreement with data published in the current literature.

Breakdown Phenomena in Rare and in Molecular Gases Using Pulsed Carbon Dioxide Laser Radiation

by

Peter Behrens
Lieutenant Commander, Federal German Navy

Submitted in partial fulfillment of the requirements for the degree of

MASTER OF SCIENCE IN PHYSICS

from the

NAVAL POSTGRADUATE SCHOOL
June 1974

ABSTRACT

Light from an atmospheric pressure, double-discharge CO_2 laser was focused in monatomic and in diatomic gases at pressures from 0.01 atm to 10 atm in order to produce optical breakdown. The gases under investigation were Ar, He, N_2, H_2, and air. Measurements of the transmitted laser intensity were obtained and the properties of the resulting spark were studied by means of an open face camera and spectroscopic techniques. For all gases studied the threshold power density was on the order of tens of gigawatts per square centimeter and decreased with increasing focal volume or gas pressure. The theoretical model was based on classical microwave cascade theory. The importance of loss terms other than electron diffusion loss was discussed. In the presence of preionization the threshold was on the order of hundreds of megawatts per square centimeter and showed no volume dependence. Emission spectra consisted of a strong continuum superimposed with strong lines due to neutral and ionized atoms. Results of this study were in good agreement with data published in the current literature.

TABLE OF CONTENTS

ACKNOWLEDGEMENT

I wish to thank Mr. Hal Herreman for assisting in the maintenance of the laser system and for his helping hand in some of the experiments. I would like to extend my sincere gratitude to Professor Cooper and Professor Schwirzke for their most helpful comments and suggestions throughout the experiments and their assistance to put the experimental results and their interpretation into words.

This research was supported in part by the Office of Naval Research, project number 099 - 400, project order PO 4 - 0077.

I. INTRODUCTION

The interaction of a high power laser beam with a plasma is of interest not only from the point of view of generating a plasma, or of laser weapons and their countermeasures, but also of a possible means of heating plasma to thermonuclear temperatures. This application attacks one of the major unsolved problems preventing achievement of fusion power. At the present time, one crisis facing our society is the socalled "energy crisis", which is the gap between the availability and the demand for clean and cheap energy. As a consequence, nowadays there is a growing emphasis on the search for new energy resources. One important area of physical research today is the laser-induced controlled thermonuclear fusion, which promises a relatively clean and almost inexhaustible supply of energy. The lowest self-sustained thermonuclear burn is the deuterium-tritium (DT) reaction in which a deuterium plasma is heated to a sufficiently high temperature. Laser heating of a confined plasma column or a laser triggered fusion microexplosion can eventually produce the high temperatures needed for this process. In recent years, there has been considerable work done on the interaction of high-intensity pulsed laser beams with gaseous and solid targets. The irradiation of solids by ruby and glass lasers has been motivated to a large extent by a desire to create plasmas of thermonuclear interest.

Some disturbing aspects of the use of such lasers are the very low efficiency (less than 1%), the high cutoff density and the relatively high cost. With the appearance of the high-efficiency TEA CO_2 lasers in the late 1960's these problems could be solved as can be seen from some typical high power pulsed laser characteristics shown in Table I [Ref. 1].

TABLE I

Typical High Power Pulsed Laser Characteristics

Laser	Nd-Glass	CO_2
Wavelength (cm)	1.06×10^{-4}	10.6×10^{-4}
Cutoff Density (cm^{-3})	10^{21}	10^{19}
Output Energy (joules)	100-1000	100-1000
Pulse Length (nanoseconds)	0.01 - 10	1 - 100
Efficiency	0.1%	10%
Cost	10^3 \$/joule	10-100 \$/joule

An intense laser pulse may cause instabilities in a plasma, thus increasing its resistivity and enhancing absorption. Theta- or Z-pinch plasma may be heated turbulently to higher temperatures than attainable by the classical

absorption mechanism of electron-ion collisions. The heating of such discharges is made attractive by using a wavelength of 10600 nm, since the cutoff density is $n_c = 10^{19}$ cm^{-3}, which is the point where the laser light frequency equals the plasma frequency. This is a density which is within reach of present high-density low-temperature pinches [Ref. 2].

Furthermore, the well known effect that gases under normal conditions are relatively transparent to electromagnetic radiation, is changed when the radiation intensity increases and reaches a certain threshold value, as happens with very high-power lasers. Gases then are no longer transparent and, as in an ordinary discharge, they become highly ionized and the transmitted radiation is greatly attenuated, thus setting an upper limit on the radiation flux density that can be transmitted through a gaseous environment. This can impose severe limitations on the use of laser beams in a large number of applications.

In order to investigate the creation of a hot dense plasma and to describe the process of growth, absorption, scattering and radiation in a controlled fashion, a laser induced breakdown of gases in a pressure cell can be used to produce the plasma. The purpose of this study was to investigate the breakdown phenomena in rare and molecular gases under pressures from 0.01 to 10 atm using pulsed CO_2 laser radiation. Of particular interest were the gas breakdown threshold measurements with 10.6 micron wavelength radiation

made in argon, helium, nitrogen, hydrogen and air. Furthermore, the threshold dependence on the focal spot size created by a focusing lens was determined. Radiation in the visible region of the spectrum from the breakdown plasma was examined spectroscopically. Laser radiation absorbed by the plasma was measured and compared to values calculated by using the kinetic theory of ideal gases and the basic theory of ionized gases, modified for the conditions in this study. Values for the plasma density and temperature were estimated and all data were compared to results published in the current literature. The theoretical analysis of initiation, expansion, radiation and loss mechanisms of a laser-induced gas breakdown was supported by the experimental results.

II. THEORY

A. GAS BREAKDOWN MECHANISM

The rapid change from transparency of a gas to intense laser radiation into an opaque highly conducting plasma takes place in four stages: initiation, growth, plasma development and finally, extinction. The initial stage is the time elapsed between the arrival of the laser radiation flash in the lens focal region and the initiation, by the release of an ion-electron pair, of the growth in the free electron and ion concentration in the gas. The initial mechanism appears to be due to multiphoton absorption, wich is the simultaneous absorption of a number of quanta of light energy from the laser beam by a single electron, so that the electron instantly receives the ionization energy and is freed from its parent atom [Refs. 3,4]. Another possible initiation mechanism could be cascade ionization, where a few initial electrons in the breakdown region are required, which in turn could be created by a process such as multiphoton ionization of the gas specie or by ionization of impurities in the gas [Ref. 5]. These electrons then gain energy by absorption from the radiation field between elastic collisions with neutral atoms. After accumulating an energy slightly higher than the ionization potential of the gas the electron may ionize an atom by inelastic collision, producing two electrons of low energy; these are then available for the

process to be repeated. Other mechanisms for initiation, though not studied extensively, are direct stripping of electrons from atoms in the electric field of the laser light wave, and tunneling of an electron through its potential barrier under the action of the high-frequency field.

The formative growth stage to breakdown is the subsequent period of amplification in the number of ion pairs until the state of "breakdown" is reached. Breakdown is defined as the attainment of a certain electron concentration (greater than 10^{15} cm^{-3}), or the degree of fractional ionization ($\delta \sim 0.1\%$) of gas atoms in the focal region which is sufficient to cause significant absorption and scattering of the laser radiation [Ref. 6]. This avalanche growth of ionization is fed by absorption of laser light. The absorption process can be considered either as an extension of microwave breakdown theory or as an inverse Bremsstrahlung process. The combined duration of the initial and formative growth times is only a few nanoseconds. Once the conditions for the onset of breakdown are satisfied there follows, if the laser intensity continues to increase, a rapid plasma development stage and the formation of a highly conducting hot expanding gas in which further absorption and hydrodynamic effects become important. Simultaneously with the breakdown occurs a bright flash of white light, in the following referred to as the "spark". Figures 1a and 1b show photographs of a typical appearance of such a spark in hydrogen and helium.

The final extinction phase lasts for a time which may be two or three orders of magnitude larger than the pulse duration of the laser, (i.e. of the order of 50 microseconds, compared to a forward halfwidth of 250 nanoseconds for the CO_2 TEA laser pulse). During this phase the plasma gradually dies away as a result of radiation emission, diffusion, attachment and recombination.

B. CASCADE DEVELOPMENT OF GROWTH STAGE

Precise theoretical predictions and measurements of the intensity of laser radiation required to create ionization and breakdown are difficult to obtain. Imprecise definition of the focal region, inaccurate knowledge of the variation of the radiation within this focal volume, uncertainties in the value of radiation power density and in the variation of the angular divergence of the laser beam are just a few examples of these difficulties. Nevertheless, considerable progress has been made and nowadays many experimental and theoretical reports give evidence in support of the view that the growth stage proceeds as a result of the cascade or avalanche mechanism of inverse Bremsstrahlung absorption, which is physically equivalent to classical excitation and ionization by inelastic collisions between atoms and electrons in which the interaction energy is drawn from the electromagnetic field of the light wave [Ref. 7]. This is essentially an extrapolation of the microwave discharge concept to optical frequencies.

Thus, once liberated in the focal region during the early part of the laser pulse by multiphoton absorption, free electrons gain thermal energy from the electromagnetic field through collisions with atoms and when their energies exceed the atomic excitation and ionization potentials they cause an amplification in the electron-ion concentration. Simultaneously occurs a loss of free electrons from the focal region due to diffusion, recombination and attachment to the electronegative atoms. If the rate of production exceeds the loss rate the concentration grows and breakdown occurs.

To discuss in theoretical terms the cascade development of gas breakdown, it appears to be appropriate to start by considering the continuity equation for the electron density:

$$(1) \qquad \frac{\partial n}{\partial t} = (\nu_i - \nu_a)n + D\nabla^2 n - \alpha_R n^2$$

where ν_i is the ionization rate, ν_a is the attachment rate, D is the electron diffusion constant, and α_R is the recombination constant. Recombination losses are usually not important in the breakdown-forming stage and hence will be neglected. In a gas breakdown experiment the laser beam is focused inside a gas cell. The focal volume can be approximated by a cylinder of radius r and length ℓ, where ℓ is larger than r. To simplify the calculation, it is assumed that the ionization rate is constant inside the focal volume during the laser pulse and the electron density is zero outside the cylinder. Equation (1) when solved, gives

$$(2) \qquad \frac{n_f}{n_o} = \exp[(\nu_i - \nu_a - D/L_D^2)T]$$

where $L_D = r/2.405$ is the diffusion length, T is the laser pulse length, and n_f and n_o are the final and the initial electron densities, respectively, in the focal volume.

For the gas to break down, a certain electron density has to be reached before the end of the laser pulse. The criterion is represented by a number k_{cr}, defined so that the number of electrons generated in a time T by a free electron is $2^{k_{cr}}$. k_{cr} is conventionally taken to be 43, corresponding to a multiplication factor of 10^{13} for each free electron in the focal volume. By equation (2), ν_i becomes

$$(3) \qquad \nu_i = D/L_D^2 + \nu_a + (k_{cr}/T) \ln 2 \quad ,$$

which, in terms of the net rate at which electrons gain energy, $d\varepsilon/dt$, and the ionization potential of the gas, I, can be written as

$$(4) \qquad \nu_i = \frac{\ln 2}{I} \cdot \frac{d\varepsilon}{dt} \quad .$$

According to the microwave theory, electrons gain thermal energy from the radiation field by elastic collisions with neutral atoms at a rate

$$(5) \qquad \left(\frac{d\varepsilon}{dt}\right)_{gain} = \frac{e^2E^2}{m} \cdot \frac{\nu_c}{\omega^2+\nu_c^2} \quad ,$$

where E is the root-mean-square electric field of radiation, m is the mass of the electron, ω is the angular frequency of the radiation, and ν_c is the electron-atom collision frequency. At the same time, electrons lose energy in elastic and inelastic collisions. In elastic collisions, the electrons simply bounce off the atom and there is some exchange of kinetic energy but no change in the internal state of the atom. The average energy loss due to such elastic collisions is

$$(6) \qquad \left(\frac{d\varepsilon}{dt}\right)_{\text{elastic loss}} = -\frac{2m}{M} \langle\varepsilon\rangle \nu_c \quad ,$$

where M is the mass of the atom and $\langle\varepsilon\rangle$ is the average energy of the electron. In an inelastic collision, there is a change in the internal state of the atom at the expense of the kinetic energy of the electron. The exact calculation of such a loss term is difficult because atoms and molecules possess many excited levels with their excitation rates not well known. Reabsorption of radiation from an excited state by a neighboring atom, if the radiation belongs to a characteristic frequency of the gas, may also occur. This phenomenon is known as resonance radiation trapping. It is also possible that the energy is eventually passed out of the focal volume and thereby lost. Due to these complications, instead of making an unreliable calculation of this energy-loss term, two characteristic parameters for it are introduced. Physically an inelastic loss term must be proportional

to the production rate of excited atoms. Once the excited state is produced, the energy may be lost in two different ways: (i) the loss is independent of the focal volume, or (ii) the loss depends on the focal volume and has a L_D^{-2} dependence. Combining these two types of losses, the energy loss due to inelastic collisions may be written as

$$(7) \qquad \left(\frac{d\varepsilon}{dt}\right)_{\text{inelastic loss}} = - \frac{I}{\ln 2} \left(\alpha + \frac{\beta}{L_D^2}\right) \nu_c \quad ,$$

where α and β are the two characteristic parameters, the first being dimensionless, and the second having dimension of $(\text{length})^2$. The factor $I/\ln 2$ introduced in equation (7) serves simplification purposes in the final resulting equation. Combining the equations (3) through (7) and defining the power threshold density as $P_{th} = (c/4\pi)E^2$, the following form for the breakdown threshold power density is found

$$(8) \qquad P_{th} = \frac{cmI}{4\pi e^2 \ln 2} \frac{\omega^2+\nu_c^2}{\nu_c} \left[\frac{k_{cr}}{T} \ln 2 + \frac{D}{L_D^2} + \nu_a + \frac{2m\langle\varepsilon\rangle \ln 2}{M \quad I} \nu_c \right.$$

$$\left. + \left(\alpha + \frac{\beta}{L_D^2}\right)\nu_c \right] \quad .$$

Equation (8) shows that the breakdown threshold in general is directly proportional to the ionization potential of the gas and passes through a minimum at the pressure when the angular frequency ω is equal to the collision frequency ν_c as indicated by the term outside the brackets. The terms

inside the brackets represent various loss terms. Depending on their relative magnitudes, the breakdown may be described as time-limited, diffusion-limited, attachment-limited or inelastic-collision-limited. Time-limited breakdown occurs if the first term in the brackets dominates, that is when the laser pulse duration is so short that the growth rate of electron density required to produce a visible discharge exceeds any losses. Then the threshold power varies inversely with the pulse length, and the breakdown is determined by product of the intensity times the pulse length, i.e., the energy per unit area.

Diffusion-limited processes occur when the second term in equation (8) dominates, i.e., the gas breakdown takes place in a small focal volume at low gas pressure. The breakdown threshold P_{th} in this case decreases as L_D^{-2} with the focal spot size and it also decreases as P^{-2} with the gas pressure in the range of pressure so that $\omega >> \nu_c$.

The third and fourth terms represent the attachment and elastic collision losses. They are relatively unimportant and the attachment loss can be completely neglected for all inert gases.

The last term in equation (8) is the energy loss due to inelastic collisions. It is important for all molecular gases because of the large number of excited states they possess.

C. EXPANSION OF THE SPARK

The expansion of the luminous spark has been studied by many authors [Refs. 8,9,10]. It has been found that the spark grows in the direction opposite to the laser light flux. This phenomenon has led to the model of a radiation-supported detonation wave. A detonation wave is a shock wave which is fed by the release of energy behind the shock front. The energy is supplied by the absorption of the incident laser beam, which is analogous to the detonation of reacting gases, with the gas reaction energy replaced by the absorbed laser energy. This absorbed energy is determined by measurements of the transmission through the focal spot. It can be shown mathematically that the velocity of expansion of the spark should increase as the one-third power of the laser energy. Experimental results [Ref. 11] are in agreement with this prediction and can be interpreted as good evidence for the radiation-supported detonation wave mechanism.

After the end of the laser pulse, the heated gas expands in the form of a blast wave, which differs from a detonation wave in that after initiation no further energy is supplied behind the shock front. A reaction occurs within some volume of gas and, as a result, the shock front propagates out through the gas, with no further addition of energy near the shock front. An analysis of the shape of the laser spark after the end of the laser pulse is based on the assumption that the spark fills the spherical sector bound by the

focused laser beam [Figure 12]. This volume expands and forms a blast wave with a perturbed spherical symmetry.

Several other mechanisms for the plasma growth have also been suggested: (i) Expansion as a breakdown wave [Ref. 8]. The light flux in the laser pulse with a rising pulse front reaches the threshold value at the focus first, exceeding the threshold value at various distances propagating backwards along the laser light path, as time goes on. The breakdown will take place in those parts of the path with a delay relative to the breakdown at the focus.

(ii) Expansion as a radiation transport wave. The heated gas emits ionizing radiation and ionizes the gas in front of the absorbing layer so that the incoming laser light will be absorbed in front of the shock wave, initiating a new breakdown region.

(iii) Expansion in the form of a travelling ionization breakdown wave [Ref. 13]. If free electrons are produced ahead of the breakdown wave by radiation from the spark, the ionization will grow backwards from the spark as described by mechanism (i). In summary it can be stated that the mechanism for the expansion of the laser spark cannot entirely be explained by one single theory, although the radiation-supported detonation wave model accounts for many features of the growth of the spark.

D. RADIATION FROM THE SPARK

Radiation is emitted from the laser-produced spark in the visible, ultraviolet, and soft x-ray regions of the light spectrum. The visible light radiated by the spark is extremely intense, of a bluish-white color and is radiated more or less uniformly into 4π steradians. Spectroscopic measurements of the sparks produced by laser breakdown of gases show in general a strong continuum along with sharp line spectra. The line width decreases with the distance from the center of the spark. In the early development of the spark an intense continuum is emitted plus some very broad lines of ionized and neutral atoms. After expansion and cooling of the spark has occurred somewhat less broadened lines from neutral atoms are emitted. One important result of spectroscopic studies is the estimation of the temperature inside the spark. Because of the high absorption of energy in a small volume, high temperatures should be produced in the breakdown region during the laser pulse. The hot plasma should then emit Bremsstrahlung and recombination radiation in the x-ray region of the spectrum. The temperatures in the spark can be determined by using different methods, such as intensity measurements of the x-ray flux emitted by the spark, line-to-continuum ratio measurements in the emitted spectrum, and plasma expansion measurements. The values obtained for the temperature in a laser spark range from 1 to 300 eV, depending on the method of determination and the experimental conditions.

Spectroscopic measurements can be interpreted to yield values for the electron density in the spark. It can be determined from the width of Stark-broadened spectral lines. For high density values, the Stark effect gives the main contribution to the line width. The electron density n_e is related to the full Stark width $\Delta\lambda_S$ by

$$(9) \qquad n_e = C(n_e,T)\cdot\Delta\lambda_S^{3/2} \quad ,$$

where the coefficient $C(n_e,T)$ is only weakly dependent on the electron density and is tabulated for many lines [Ref. 14]. The results of density measurements indicate that at early times during the creation of the spark a very dense plasma with density values larger than 10^{19} cm^{-3} is formed. The density is consistent with complete single ionization of the gas within the focal volume. As time progresses the electron density decreases rapidly. In the after glow densities in the range of 10^{18} cm^{-3} persist for about a microsecond of time. Observations of scattering of the laser beam itself by the created plasma are consistent with the theory of scattering by the free electrons in the plasma, under conditions such that the spectral distribution of the scattered radiation is governed by cooperative interactions between ions and electrons. The wavelength of the scattered

radiation is shifted slightly with respect to that of the laser beam. This is interpreted as a Doppler shift due to a motion of the plasma toward the incident beam during the initial phase of the spark. If the extent of the plasma is greater than that of the scattering volume, the fraction of the incident beam scattered away, fr_{scat}, is independent of the cross section of the beam. For scattering by free electrons this fraction is given by

$$(10) \qquad fr_{scat} = 8 \times 10^{-26} \cdot n_e \cdot \ell \cdot \Omega ,$$

where n_e is the average electron density and ℓ is the length of the beam scattered in the direction of observation of solid angle Ω [Ref. 15].

E. SELF-FOCUSING

Plasma instabilities can cause an increase in resistivity of the plasma and thus enhancement of absorption due to moderate ion density fluctuations. If the plasma frequency is close to the laser frequency a threshold power density for the onset of some parametric instabilities can be expressed as

$$(11) \qquad P \geq 10^{-10} \cdot n_e \cdot T \quad , \quad \text{[Ref. 16].}$$

Self-focussing effects in a hot dense plasma will increase this power density significantly. The phenomenon of self-focussing can be described as an interaction of the electric field of the laser beam with the index of refraction of the medium in which the beam is traveling. A very high electric field thus increases the index of refraction of the medium. Therefore, at the center of the beam the light will travel more slowly than at the edges, so that the beam tends to be focused toward the center. The same mechanism keeps the beam from diverging. This phenomenon can lead to a stable region where the light beam is trapped in a very narrow filament extending over a distance of a few microns [Ref. 17].

F. CALCULATIONS

1. Temperature Inside The Laser Spark

The following calculations are made for argon gas at a pressure of three atmospheres which is equivalent to 3.04×10^5 [N/m^2]. Using the ideal gas equation of state (12) $P = N k T$, [Ref. 18], where N is the number density in m^{-3}, k is the Boltzmann constant, and T is the temperature in degrees Kelvin, the number density of molecules in the argon gas at 288° K is

$$N = 2.52 \times 10^{20} \cdot P. \qquad (13)$$

The fully ionized argon plasma contains 4.6×10^{26} electrons per cubic meter. Gas breakdown occurs at the point that has the highest power density, that is, the focal spot.

From geometrical optics in the far field, the spot diameter in the focal plane of the lens is

$$(14) \qquad d = f \cdot \theta$$

where f is the focal length of the breakdown lens, and θ is the laser beam divergence. Using a focusing mirrow with a focal length of 140 cm the burn pattern of the laser has been measured for the NPS TEA laser and a beam divergence of 4.28×10^{-3} radians has been obtained. Using a germanium lens with a focal length of 2.54 cm, d is obtained as 10.87×10^{-5} m. In order to calculate the focal volume, in which the interaction of the laser radiation and the gas takes place, the interaction length ℓ is estimated by use of the formula for the focal depth

$$(15) \qquad \ell = 4 \lambda (f/\Delta)^2 ,$$

where λ is the wavelength of the laser, f is the focal length of the focusing germanium lens, and Δ is the unfocused laser beam diameter of the optical system. With Δ equal to 1 cm, ℓ is 2.74×10^{-4} m. Thus the calculated focal volume is 2.54×10^{-12} m^3. In this initial plasma volume there are 1.17×10^{15} electrons and the same number of protons. With a laser pulse energy of 1 joule the resulting energy density is 3.94×10^{11} J/m^3, and each electron will receive 8.56×10^{-16} joules or 5353 eV. Compared to values found

in the current literature this value is too high by a factor of ten to one hundred. This has to be the case since the dynamics of plasma expansion and background heating, which both are initiated while the laser is still radiating, have not been accounted for in the above calculations. A.A. Offenberger and N.H. Burnett [Ref. 19] used a single-mode CO_2 laser pulse of approximately 10 MW peak power. For hydrogen at 700 Torr they found an initial plasma temperature of approximately 65 eV.

2. Electron Densities In The Spark

The idea of anomalous heating of a plasma by a laser beam has been proven in computer calculations and recent laboratory experiments by different authors. This anomalous heating is a result of moderate ion density fluctuations which give rise to strong enhancement of high frequence resistivity at frequencies in the vicinity of the plasma electron frequency. This enhancement in high frequency resistivity yields an increased absorption in the plasma and thus a heating up to thermonuclear temperatures. The electron plasma frequency is given by the equation

$$(16) \qquad \nu_{pe} = \frac{\omega_{pe}}{2\pi} = \frac{1}{2\pi} \cdot \frac{n_e \cdot e^2}{m \cdot \varepsilon_o} = 8.99 \times 10^3 \cdot n_e^{\frac{1}{2}} ,$$

where n_e is the electron density in cm^{-3}, e is the elementary charge, ε_o is the permittivity of free space, and m is the electron mass. The frequency of the CO_2 laser is 2.83×10^{13} sec^{-1}. Since the intense electric fields

experienced in the laser beam might be sufficient to obtain the above stated ion density fluctuations in the vicinity of the plasma electron frequency, the laser frequency is set equal to the electron plasma frequency and solved for the electron density, thus yielding a value of

$$(17) \qquad n_e = 9.9 \times 10^{18} \text{ cm}^{-3}.$$

3. Absorption Of Laser Radiation In The Spark

The absorption of the incident laser radiation by the plasma can be described by Lambert's law. Energy is absorbed over a distance L according to the equation

$$(18) \qquad W = W_o (1 - e^{-KL}),$$

where W_o is the laser output energy, K is the absorption coefficient, and L is the absorption length. When the plasma frequency is close to the laser frequency the classical absorption length is according to Kaw, et al. [Ref. 20]

$$(19) \qquad L = 5 \times 10^{18} T^{3/2}/n_e \quad \text{(in micrometer)}$$

where T is measured in electron volts. Assuming an electron temperature of 65 eV and using the value for the electron density calculated above, the absorption length is 2.65×10^{-4} m, which is about equal to the interaction

length ℓ, calculated with Equation (15). From measurements taken with an open face camera the actual length of the created plasma column was found to be approximately 4×10^{-3} m. Absorption in the spark is assumed to proceed via inverse Bremsstrahlung for which previous experimental work [Ref. 21] has established an effective energy absorption coefficient given by

$$K = 1.8 \times 10^{-35} \left(n_e^2 / T_e^{\frac{3}{2}}\right) \left[cm^{-1}\right] , \tag{20}$$

with T_e in eV, and n_e in cm^{-3}. Using the above values for the electron density and temperature, K is calculated to be 3.37 cm^{-1}. Inserting this value for K together with an estimated interaction length of 0.4 cm into Equation (18) the value for W becomes 0.7402 and thus about 74% of the incident laser energy is absorbed by the created plasma. In the current literature [Ref. 15, 22] absorption values of 65% are stated for spark production in air. The difference is due to an estimated interaction length of 0.3 cm. From the remaining laser radiation about 2% is scattered and reflected by the plasma and the rest is being transmitted.

III. EXPERIMENTAL PROCEDURE

A carbon dioxide (CO_2) Transverse Excitation at Atmospheric pressure (TEA) laser built by Nat M. Ceglio and Ronald F. Bishop in 1972 was used throughout the study. This laser system consisted of a resonant cavity, a Tachisto Marx generator, a pulse shaping network composed of passive electrical components, a D.C. power supply and a gas flow system. The laser box was a rectangular container, 40 inches long, 12 inches wide, 6 inches high, and was made of 1 inch thick acrylic lucite walls. The ends of the laser box consisted of two NaCl crystals serving as Brewster windows. Inside the box the electrode assembly, consisting of parallel anode and cathode plates, each 38 inches long and 5 inches wide, and a row of 144 trigger electrodes, was located. Although carbon dioxide is the gas which after sufficient excitation emits coherent radiation in a CO_2 TEA laser system, nitrogen and helium are also important in promoting efficient laser radiation. The preionization and glow discharge as well as the laser output power and efficiency depend upon the component ratio of the gas mixture. The gas flow was made up of a mixture of CO_2, helium, and nitrogen gases using a ratio of 85% helium, 7.5% CO_2, and 7.5% nitrogen in a flow rate of approximately 1 ft^3/minute. With this mixture a laser pulse similar to that shown in Figure 10 was obtained.

A CO_2 TEA laser depends upon selective direct electron impact and molecule-to-molecule energy transfer for creation of the population inversion necessary for laser output. Both of these processes occur when the gas mixture is subjected to electrical breakdown between the electrodes within the laser cavity. Atmospheric pressure operation is preferable to low pressure operation due to the greater molecular density and, therefore, greater available energy. Transverse excitation implies a short discharge length but a large discharge area to achieve the discharge volume necessary to excite the gas mixture, create a population inversion, and enable lasing action to occur. Small working voltages and the low impedance of a small electrode gap allowing rapid injection of the discharge excitation energy, make the transverse excitation superior to longitudinal excitation. Double-discharge preionization techniques are used in conjunction with a transverse excitation in order to attain a uniform volume discharge. Preionization was accomplished through the use of 144 insulated trigger electrodes charged to the same potential as the anode. A three-stage Marx generator supplied with a negative voltage up to 22 kilovolts and 15 milliamps by an unregulated D.C. power supply was used as the electrical power source for the breakdown. Since a voltage multiplication by three was achieved in the Marx generator, a lower charging voltage was used to attain up to 66 kilovolts to produce the atmospheric pressure breakdown between the laser electrodes.

The uniform glow discharge produced by the double-discharge system was an effective pumping mechanism for exciting the gas mixture. A glow discharge between the electrodes can be maintained by limiting the discharge time such that it is short compared to the arc formation time. For proper operation, it is necessary to generate a glow discharge in the large discharge volume then reduce the voltage enough to prevent arc formation. Control of the voltage rise time and decay time constants of the input energy pulse from the Marx generator to the laser cavity electrodes was effected through the use of a pulse shaping network of passive circuit elements consisting of a combination of resistors, inductors, and capacitors (see Ref. 34).

In addition to the population inversion of a lasing medium (CO_2 molecules), a resonant cavity consisting of two mirrors and the discharge volume of the laser box is required for laser output. The two mirrors form an optical resonator. The back mirror was a 4" - diameter polished copper mirror with a three meter radius of curvature, and the front mirror was a 4.5" - diameter germanium mirror, which was partially transmitting to allow a fraction of the laser radiation energy to escape as output. The total laser energy in such a typical output pulse (see Figure 10) was approximately one joule. The laser energy in the initial spike, which occurs during the time of current flow in the laser discharge resulted from the pumping of the CO_2 molecule lasing level

by electron impact. The remaining energy, occurring well after the termination of the laser discharge current, resulted from pumping of the CO_2 by the excited N_2 - CO_2 inelastic collisions.

Some important characteristics of the laser system are listed in Table II.

TABLE II

Important Characteristics of the CO_2 TEA Laser System

Energy	up to 10 joules
Pulse Width	250 nanoseconds
Peak Output Power	15 to 18 megawatts
Wavelength	10.6 micrometers
Beam Diameter	2 cm
Maximum Input Voltage	66 kilovolts
Laser Efficiency	5 to 10% minimum

A pressure cell made of aluminum, shown in Figure 2, was constructed and used to contain helium, argon, nitrogen, hydrogen, or air gas at pressures ranging from 0.01 to 10 atmospheres. The center cavity of the cell had a volume of 720 cm^3. The specific construction of the cell was chosen

in order to obtain viewing angles of zero, 45, 90, and 135 degrees with respect to the created plasma.

The two inch diameter entrance and exit windows were made out of potassium bromide (KBr). Typical spectral data for potassium bromide are shown in Figure 3. The side windows, also two inches in diameter, were of either potassium bromide or Pyrex 7913 tempered glass, depending on the specific experimental setup. The top of the cell contained openings for the gas in- and outlet, a pressure gauge, a vacuum pump connection, and a cylindrical alumina (Al_2O_3) rod (0.635 cm diameter), serving as a reference mark inside the cell. Whenever hydrogen gas was used, the cell was purged with nitrogen gas first, then evacuated with a forepump in order to insure a safe operation. The laser beam traveled through a circular aperture of 5.7 cm diameter, whose purpose will be explained in the data section, and a rock salt flat which served as an 8% beamsplitter, to a polished copper mirror with a focal length of 140 cm guiding the beam towards the entrance window of the pressure cell. The beam was focused at the center of the cell with either a 2.54 cm focal length double convex coated germanium lens (L_1), or with a 12.7 cm focal length planoconvex coated germanium lens (L_3), mounted in front of the entrance window. Germanium was chosen because it is a good material for use in transmitting components for several reasons: (i) It has a high thermal conductivity which allows efficient cooling and reduces the chance of damage at high power

operation. (ii) It has a relatively low absorption. At 10.6 microns the absorption of germanium is dependent on purity and temperature. The germanium used for optical applications absorbs between 0.7% and 1% per mm. (iii) Germanium can be polished and coated to a very high quality optical finish. Table III below shows some typical material properties of germanium.

TABLE III

Material Properties of Germanium

Refractive Index at 10.6 microns	4.0
Specific Heat (cal/g °C)	0.074
Density (g/cc)	5.33
Thermal Expansion Coefficient (10^{-6}/°C)	6.1
Thermal Conductivity (cal/cm sec °C)	0.14

Typical spectral data for germanium are shown in Figure 4 [Ref. 23].

At the exit window of the pressure cell a second germanium lens (L_2) of the same type as lens L_1 was used to focus the diverging forward scattered laser light to the entrance window of a photon drag detector, connected to a Tektronix 545 A oscilloscope. In this fashion the pulse shape of the transmitted laser pulse was monitored and, after integration, peak values for the laser output power

were obtained. In a photon drag detector the radiation enters and passes down through the detector element, a bar of doped germanium crystal. Photons in the incident beam transfer their momentum to free carriers in the germanium (holes in p-type or electrons in n-type germanium). The free carriers are physically driven down the bar by the energy loss from the photons, thus creating a voltage gradient which is either amplified or fed directly to the output socket of the instrument. Some important specifications of the photon drag detector are given in Table IV:

TABLE IV

Specifications of the Photon Drag Detector

Response Time	less than 1 nanosecond
Responsivity at 10.6 microns	0.18 ± 0.1 mV/KW
Output Resistance	50 ohms
Operating Temperature	Room Temperature

Intensity measurements of the laser created spark light were taken using a UDT PIN 10 photodiode as a detector looking through the 90° side window of the pressure cell. The measurements were displayed on a second Tektronix 545 A oscilloscope. Pictures from both scopes were taken with polaroid cameras providing instant readout.

The spark light in the visible spectrum scattered 90° was also investigated with a spectrograph, looking through one of the side windows of the pressure cell. Inside the spectrograph light was focused through a 39.5 cm focal length lens onto a vertical slit. The slit was imaged on an optical grating having 1200 grooves per mm and a blaze angle of 36° 52'. From this grating the light was refocused by an AEROSTIGMAT 305 mm focal length lens onto a film holder containing a sheet of KODAK Super-XX Pan film, a high speed panchromatic film with an ASA value of 200. The energy in each laser pulse was determined by splitting off 8% of the laser beam with a rocksalt flat beamsplitter and sending this reference beam to a 1 m focal length polished copper mirror (Mirror 2). By this mirror the reference beam was focused onto the sensitive area of a Ballistic Thermopile, connected to a microvoltmeter. A schematic drawing of the experimental setup is shown in Figure 5, whereas Figure 6 shows a photograph of the actual equipment used throughout the study.

The Ballistic Thermopile is a calorimetric device that measures the temperature rise due to absorbed radiation. It consists of two nickel-plated cones (receiver and reference) and series-connected iron-constantan thermocouples. The thermocouples are arranged so that the hot junctions are attached to the receiver cone and the cold junctions to the reference cone. Radiant energy is directed to the entrance hole of the receiver cone, where it is

almost totally absorbed due to the Mendenhall wedge (multiple relections) effect. The temperature rise of the receiver cone with respect to the reference cone causes an emf, which is then monitored by the externally connected microvoltmeter. The peak emf measured is linearly related by the calibration factor to the total input energy. Because of its high reflectivity, the receiving surface of the receiver cone resists the destructive effects of high peak power pulses encountered in laser work. Some important characteristics of the Ballistic Thermopile are given in Table V:

TABLE V

Characteristics of a Ballistic Thermopile

Ballistic Time Constant	50 seconds
Equivalent Noise Level	300 microjoules
Maximum Energy Input	1000 joules
Maximum Power Input	10^9 watts
Sensitivity	35 microvolts/joule
Output Impedance	100 ohms
Measurement Error	less than 5%

A Speed Graphic still picture camera with a focal length of 127 mm equipped with a Polaroid film back was used to obtain pictures of the laser created breakdown spark in the focal region of the focusing lens inside the pressure cell.

The camera was focused on the reference rod in the center of the cell. The rod was placed far enough away from the developing plasma as not to interfere with the expanding plasma cloud. The camera was placed to look into the cell at an angle to the normal of the window plane in order to separate the actual plasma image from window reflections.

The optical alignment of the system was checked daily since it was sensitive to vibrations caused for example by a truck driving by the plasma laboratory. It was sufficient to check the alignment of the laser back and front mirror by recording their micrometer position readings since the complete laser cavity was mounted on the same optical bench. The position of the entrance window of the pressure cell was verified by placing a piéce of footprint paper over the entrance, firing a laser shot and recording the position of the burn pattern relative to the entrance window. The position of the thermopile had to be checked with a sensitive surface illuminated by an ultraviolet light source, thus imaging the low intensity 10.6 micron-radiation of the reference beam. All potassium bromide windows, the rock salt beamsplitter and the two Brewster angle rock salt entrance and exit windows of the laser cavity had to be illuminated by a light bulb, whenever the system was not in use, in order to avoid extensive fogging. After several months of use these hygroscopic materials had to be cleaned and polished to guarantee efficient laser operation. As safety precautions goggles had to be worn at all times when

the laser was in operation, and the Marx generator capacitors had to be discharged with a grounding bar after termination of the daily experiments.

IV. DATA

A. MACROSCOPIC PROPERTIES OF THE PLASMA

The data in this study were taken mainly in two areas of interest: (i) investigation of macroscopic properties of the plasma created by laser-induced gas breakdown, its initiation and growth, and (ii) spectroscopic studies of the microscopic properties of the plasma.

1. Beam Quality Measurements

Preliminary work had to be done in order to improve the beam quality of the CO_2 laser system. Measurements in the far field indicated that the laser beam mode pattern consisted of several asymmetrical modes resulting in an uneven burn pattern containing several hot spots. Apertures of different shapes and sizes were tried out and a circular aperture with a diameter of 5.7 cm finally chosen, thereby obtaining a near-circular beam spot of almost uniform intensity with a diameter of 0.6 cm. In most of the gas breakdown experiments performed the beam was focused by a short-focal-length germanium lens. If the laser is operating with several competing modes, the local fields in very small volumes can be much larger than the value averaged over the entire focused volume. At low gas pressures up to 10 atmospheres and for cascade ionization, electrons diffuse rapidly from small regions of large fields and become distributed over the entire focused volume. Therefore, it

was assumed that the influence of nonuniform field distribution effects were of little importance in the experiments.

2. Measurements of Laser Light Absorption

One of the most impressive phenomena observed throughout the experiments was the extinction of the laser light by the breakdown region. This strong absorption together with the occurrence of the typical bright flash of white light (see Figure 1) was used in all measurements as a critical test of whether breakdown had actually occurred. The oscilloscope trace of Figure 7a shows the shape of the original laser pulse of approximately 2 joules energy and Figure 7b shows the shape of the pulse transmitted through the plasma when breakdown occurred at an energy slightly higher than 2 joules. Both traces of the forward scattered laser radiation were obtained with the photon drag detector using nitrogen gas at a pressure of 1 atm. At early times in the laser pulse there was no attenuation, but after breakdown occurred, the plasma became very opaque. This very abrupt shutoff of the transmitted light, shown in Figure 7b as a very sharp spike, occurred approximately 200 nanoseconds after the initiation of the spark. Forward transmission of the laser light was studied for a series of pulses with increasing input energy. By means of the UDT PIN 10 photodiode which was placed at one of the 90° side windows of the cell, the intensity of the spark light was recorded (Figure 8a) simultaneously with measurements of the forward transmitted laser light (Figure 8b). From a

series of pictures showing the spark light intensity (see Figure 8a) the growth time of the spark was determined to be less than 250 nanoseconds. As the laser irradiance increased, breakdown occurred earlier in the pulse. Data for time-to-breakdown as a function of peak irradiance for various background gases are plotted in Figure 9. Time of breakdown was defined as the point at which strong absorption started. Several pictures showed that the breakdown did not start until after the peak of the laser pulse. This is strong evidence for the influence of the growth of the cascade on the observational results and that the entire process does not occur by the mechanism of multiphoton absorption, explained earlier.

The percentage of total laser energy transmitted through nitrogen gas at 3 atm pressure with and without the occurrence of breakdown absorption is shown in Figure 10, which shows that the transmitted light intensity falls to zero rapidly as the plasma grows to cutoff density. The area under the curves resulted in a transmission value of the total input energy of 23.8%, which means that 76.2% of the incident laser light is consumed in the spark. This is consistent with the absorption value computed in the theory section by equation (18). The difference of about 2.2% accounts for scattering and reflection losses, since the total loss of energy consists of absorption, scattering and reflection of laser light by the plasma. Values for the amount of radiation scattered and reflected by the plasma,

found in the current literature (see Refs. 19, 22) were approximately 2% of the total incident laser energy.

To prove the fact that the breakdown of a gas has indeed a definite threshold the transmission of argon gas at 3 atm pressure as a function of peak output power of the laser was measured and is plotted in Figure 11. It shows the integrated energy transmitted, including total transmission up to the breakdown point and extinction after. The transmission of the argon gas dropped sharply to a value below 30% and the curve flattens out at about 20%, corresponding to the fraction of energy transmitted before breakdown occurred.

The peak value of the laser output power P_{Lmax} plotted against the total laser output energy is shown in Figure 12. These data for P_{Lmax} were obtained by N. Ceglio [Ref. 24] using a reliable calibration for the photon drag detector, by integrating the power signal and equating it to the total measured output energy. For values of energy below 0.5 joules the corresponding peak power values are approximations since the photon drag signal-to-noise ratio became very poor at low energy values. The general shape of the P_{Lmax} curve shows how the laser output pulse shape progresses as the laser pulse energy was increased. At low output energies the pulse shape was rather broad but it sharpened up as the energy was increased putting much of this increased energy into the first peak of the laser pulse (see Figure 10), thereby increasing P_{Lmax}. However,

an increase of the energy beyond the inflection point broadened the tail of the laser pulse without adding appreciably to an increase of its peak power.

In order to obtain values for the peak irradiance, the area of the focal region for the lenses used throughout the experiment had to be determined. Three different lenses were used as a focusing lens at the entrance window of the pressure cell: (i) a 2.54 cm focal length biconvex germanium lens, (ii) a 12.7 cm focal length planoconvex germanium lens, and (iii) a 10 cm focal length planoconvex arsenic trisulphide lens. Transmission characteristics for arsenic trisulphide glass are shown in Figure 13 [Ref. 25]. Using equation (14) with a beam divergence value of 4.28×10^{-3} radians, the following values for the focal spot diameters were computed:

1-inch germanium	1.087×10^{-4} m
5-inch germanium	5.436×10^{-4} m
10-cm arsenic trisulphide	4.280×10^{-4} m .

It was found that for a small focal volume a higher laser intensity was required to produce breakdown within the same time. This can be explained by a loss mechanism in the cascade process. Buildup of the cascade process is limited for small focal volumes by losses due to radiation or electron diffusion out of the focal region. For a larger focal volume the cascade process grows more rapidly for a given irradiance.

3. Breakdown Threshold Measurements

a. Purity of Background Gases

The development of gas breakdown by cascade multiplication of free electrons was of primary interest in this study. For cascade multiplication to be initiated, there had to be at least one free electron in the focal volume of the converging lens at the time that the laser is radiating. It was found throughout the experiments that the background gas was much more difficult to break down whenever a new gas was introduced into the pressure cell. However, once gas breakdown had started, without changing the gas in the cell, it was rather easy to continue the breakdown at much lower input energies. One explanation for this observation could be the fact that once the gas had broken down, a large number of electrons were produced in the focal volume, from which a small number of residual electrons remained in the focal volume even 10 to 30 seconds after breakdown production. Another explanation could be that during the development of gas breakdown, long-lived molecular species were produced having possibly very low ionization potentials. Thus, for a subsequent laser pulse, electrons are immediately available. Measurements carried out using the technique described above corresponded to the measurement of cascade ionization threshold of preionized gases and were carried out for comparison purposes mainly throughout this study. To avoid preionization of the gas the following procedure was used.

Whenever breakdown had been achieved, the gas outlet valve of the pressure cell was opened, the cell was flushed with new gas, evacuated with the vacuum pump and finally refilled with new gas, thus ensuring the use of unpreionized gas. However, it has to be stated, that the purity of the gases used is very critical for the data obtained, since impurities in the original gas or driven into it from the cell walls by the laser beam would provide a preionization and thereby influence the experimental results [Ref. 26]. Relative purity of the background gases used was therefore assumed throughout the study.

b. Threshold Dependence on Background Gas Pressure

Single laser shots were fired into the pressure cell and the power output after each shot was changed until breakdown occurred. The breakdown threshold was defined to be the power at which gas breakdown occurred on approximately 50% of the laser shots. The gas breakdown threshold is dependent on the pulse shape of the laser; however, the pulse shape did not vary significantly within the energy range used in the experiments. Therefore, any influence on the breakdown threshold due to pulse shape alteration has been neglected.

In Figure 14 the breakdown threshold in watts per square centimeter as a function of pressure in atmospheres for argon, helium, hydrogen, nitrogen and air is plotted for a focal spot diameter of 1.087×10^{-2} cm (1-inch germanium lens). The pressure dependence of the rare gases

is different from that for the diatomic gases, which is in agreement with data found by R. Minck [Ref. 27] in the case of a ruby laser breakdown. For argon and helium the threshold in the pressure range from 0.01 to 10 atm was found to vary as $p^{-1/5}$ with respect to pressure, whereas for nitrogen and hydrogen the threshold varied as $p^{-1/2}$ and $p^{-1/3}$ respectively (see Figure 14). A distinct minimum was observed at a pressure of four atmospheres for nitrogen yielding a threshold value of 2.1×10^{10} w/cm^2, and for hydrogen at a pressure of 7 atmospheres with a threshold value of 1.65×10^{10} w/cm^2. Figure 16 shows a comparison plot of data obtained in this study with those obtained by G.A. Hill et al., [Ref. 28] and data found by D.H. Gill and A.A. Dougal [Ref. 36] for nitrogen gas. It shows that the data found in this study are in good agreement with the data obtained by G.A. Hill who used a CO_2 laser in the same power range as the system used in this study. D.H. Gill used a ruby laser and obtained a distinct minimum for nitrogen at around 100 atm. No explanation for this difference is apparent.

c. Threshold Dependence on Focal Spot Dimensions

The breakdown threshold was also examined as a function of the focal spot dimensions, using the three lenses of different focal lengths described earlier. Figure 16 shows the breakdown threshold for argon at a pressure of 6 atm as a function of the characteristic focal dimension Λ. In this figure, Λ gives the average dimension of the focal

volume, assumed to be a cylinder of diameter D and of length L. Λ was computed with the equation

$$(21) \qquad \frac{1}{\Lambda^2} = \left(\frac{4.8}{D}\right)^2 + \left(\frac{\pi}{L}\right)^2 ,$$

and results are shown in Table VI below.

TABLE VI

Computation Of The Characteristic Focal Dimension

Lens Type	D (in meter)	L (in m)	Λ (in m)
1-inch germanium	1.087×10^{-4}	2.54×10^{-4}	2.18×10^{-3}
10-cm arsenic trisulphide	4.280×10^{-4}	8.50×10^{-4}	8.46×10^{-3}
5-inch germanium	5.480×10^{-4}	1.06×10^{-3}	1.08×10^{-2}

As can be seen from Figure 16 the threshold decreases rapidly with increasing focal dimension Λ, indicating that the loss process controlling breakdown is reduced by increasing the dimensions of the breakdown leading to a reduced threshold. The focal-dimension dependence observed could be the result of beam trapping in the neutral gas, where the longer focal lengths increase the length over which the intensity is sufficiently high that the beam self-focusses. This explanation is further supported by pictures taken with the open face camera through one of the 90° side windows of the pressure cell from a plasma created by the 5-inch focal

length germanium lens in hydrogen at a pressure of 3 and 6 atm. These pictures, shown in Figures 17a and 17b, indicate that breakdown occurred in many very small regions with subsequent expansion from these isolated centers, rather than in one big area of interaction. The most reasonable explanation for this effect is the occurrence of self-focussing prior to breakdown, with the observation of several breakdown regions being attributed to the existence of several self-focussing points. Very similar experimental results have been obtained by V.V. Korobkin and R.V. Serov [Ref. 29] in liquids.

d. Threshold Dependence on Focal Spot Dimensions for Preionized Gases

In Figure 18 the breakdown threshold dependence is plotted as a function of the characteristic focal dimension Λ in the case of preionized argon and helium. The data show that for a preionized gas the threshold had essentially no focal volume dependence. This is because at high electron densitites the diffusion processes were ambipolar and the diffusion time was long, even for small focal diameters. For this situation the threshold is determined only by the amount of energy required to ionize all gas atoms in the focal volume during the laser pulse time.

e. Threshold Dependence on Frequency

A comparison between the obtained value for argon gas at 6 atm pressure with data from H.T. Buscher, et al., [Ref. 37] who used 1.06-micrometer radiation from a Nd-glass

laser and 0.6943-micrometer radiation from a ruby laser and the second harmonics of each, yields the following values:

Wavelength (in micrometer)	Breakdown Threshold
10.6	2.69×10^{8} w/cm^2
1.06	4.9×10^{9} w/cm^2
0.6943	2.5×10^{10} w/cm^2
0.5300	2.7×10^{10} w/cm^2
0.3470	6.2×10^{9} w/cm^2

At low values of frequency, the breakdown threshold increases with frequency. For gas breakdown induced by classical microwave fields the threhold intensity is proportional to the square of the frequency, provided that the frequency is much greater than the electron collision frequency. It is expected, however, that when the photon energy becomes very high, comparable to the excitation energy of the gas, this behavior will no longer be followed.

f. Discussion Of Experimental Results

By studying the data obtained for the dependence of the breakdown threshold on the focal volume and on the gas pressure, it was possible to clarify the breakdown mechanism and to weight the importance of various loss terms. According to Equation (8), diffusion-dominated breakdown at microwave frequencies shows a pressure dependence of p^{-2}, whereas the data shown in Figure 14 indicate a much weaker dependence between $p^{-1/2}$ and $p^{-1/5}$. This

indicates that the free-electron diffusion cannot be the dominating loss term. The inelastic collisions must also be important, especially for diatomic gases. In hydrogen and nitrogen the pressure dependence does not follow simple cascade theory and this could be attributed to the effect of vibrational excitation. A combination of diffusion losses and losses due to inelastic collisions will still give a strong focal-dimension dependence but a weaker pressure dependence between p^{-2} and constant, depending on the size of the focal volume. The other three loss terms in Equation (8) will also contribute but they are relatively unimportant. The experimental evidence indicates that the dominating loss mechanism is not electron diffusion [Ref. 30]. The time required for an electron to diffuse out of the focal volume during the cascade time of less than 250 nanoseconds would require a focal spot size of 10^{-2} cm or smaller (see Ref. 26). The importance of the diffusion also decreases nearly as the square of the focal dimensions (see Figure 16). Furthermore, the diffusion loss would decrease as the pressure increases. Therefore, the dominating loss process must be a fast process, faster than free-electron diffusion, exhibiting the focal-dimension dependence similar to diffusion. Without making a quantitative analysis, the atomic-excitation resonant-radiation-trapping discussed by D.C. Smith [Ref. 31] is considered a possible dominating loss mechanism. Here, an electron excites an atom and the excited atom

loses the excitation energy by a radiative transition. In small focal dimensions this excitation energy is lost to the breakdown process. By increasing the focal diameter, a higher probability exists for resonant radiation trapping and thereby less energy loss occurs. This then leads to a lower breakdown-threshold intensity.

B. SPECTROSCOPIC STUDIES

Studies of microscopic properties of the plasma were aimed to give more detailed information on properties such as densities and temperatures of electrons as well as their expansion velocities. Since it is difficult to introduce any material probe into a small plasma, spectroscopic methods appear to be most promising.

The breakdown spark in all gases investigated was viewed normal to the laser axis with the slit of the spectrograph also at 90° to the laser axis. A wavelength calibration spectrum was obtained from a mercury arc lamp and is shown on all spectrograph pictures below the breakdown spectrum of the gases under investigation (Figures 19 through 24). For each examined background gas fifty laser shots, each creating a spark, had to be fired into the pressure cell without flushing in between, in order to obtain an image of the spectrum on the KODAK Super-XX Pan film. Furthermore, the slit of the spectrograph had to be opened quite a distance to get sufficient light intensity on the film. Spectra

were taken in argon, helium, nitrogen, hydrogen, and air using a spectral range from 4000 to 6000 angstrom.

The argon spectrum, shown in Figure 19 is typical of that obtained with monatomic gases. The breakdown spark is characterized by a strong continuum with strong lines superimposed due to neutral and ionized atoms. The wavelengths of the spectral lines were calculated with the use of the Hartmann dispersion formula described in detail in Appendix A. The brightest lines in argon are neutral atomic lines at 4510 Å and 4354 Å; significant lines of ionized atoms are 4879 Å, and 4806 Å. Exact measurements of the line width and comparison by the method of Stark broadening in order to obtain values for the electron density of the plasma could not be carried out since the resolution capability of the spectrograph was not high enough.

Figure 20 shows the emission spectrum from laser-excited nitrogen. It consists mainly of line radiation due to nitrogen atoms and ions. A nitrogen spectrum obtained from a Geissler tube would be characterized by molecular bands, which are missed completely in a laser spark spectrum. In a Geissler tube the electron temperature is very high, whereas the translational temperature of the large particles is very low. Thus, the absence of molecular bands and the presence of many atomic lines in a spark spectrum may indicate that the gas temperature in the breakdown spark is also very high.

The intensities of the lines, taken from spectral tables [Ref. 32] are indicated by the number in parentheses and the respective ionization potential for the spectral line is given in electron volts. The brightest lines in nitrogen were at 4447 Å, 5001 Å, and 5686 Å, all due to singly ionized nitrogen atoms (N II). The spectral range between 4000 Å and 6000 Å has been extensively studied to determine if the doubly ionized nitrogen (N III) spectrum was excited. Strong N III lines are listed to be at 4097 Å, 4200 Å, 4379 Å, and 4640 Å. Most of these lines of the N III spectrum will be difficult to detect since they are overlapped by N II lines. Furthermore, these lines will be buried in a strong continuum. For a laser peak power of 1.1 megawatts the expected N III lines could not be detected (Figure 20). Figure 21 shows the same kind of spectrum for nitrogen, obtained with a laser peak power of 2.6 megawatts. This spectrum shows an additional, though very weak, line at 4640 Å, which is a line for doubly ionized nitrogen. It is relatively free from overlap with N I and N II lines and has an ionization potential of 33.11 eV. The absence of molecular spectra and some evidence of a threshold for the appearance of doubly ionized nitrogen indicate that the plasma may be in a state of near equilibrium at a high temperature [Ref. 33]. Figure 22 shows a spectrum of helium and consists of only two intense atomic lines at 4471 Å and 5875 Å, where the former is much more intense, which is the reason for the pinkish-blue color of the breakdown spark observed in helium.

The emission spectrum for hydrogen is shown in Figure 23. It consists of a fuzzy continuum around the line at 4861 Å which is the second strongest line in the Balmer series arising from the transition between the fourth and the second energy level of hydrogen atoms. The gas pressure used for this spectrum was 10 atmospheres and the slit width had to be increased even further in order to get an image on the photographic film. Thus, pressure broadening plus an extensive slit width might have been the reason for the broad spectrum obtained, rather than getting a sharp line spectrum containing a single 4861 Å line.

Figure 24 shows a typical spectrum obtained in air. The lines in this spectrum belong to atomic and singly ionized nitrogen and oxygen atoms. The brightest lines shown are for singly ionized nitrogen atoms at 5001 Å, 5679 Å and for neutral atomic oxygen at 5958 Å. In general, the incident laser pulse contained many times the energy required to ionize all of the gas atoms within the volume occupied by the plasma. While only a small fraction of the incident laser light is converted to visible and uv emission from the plasma, this emission, particularly in the vicinity of the sharp line spectra, is extremely intense and could itself be useful as a light source. Its spectral radiance exceeds that of a flashlamp used to pump a laser.

V. RECOMMENDATIONS

During the study the very intense radio-frequency radiation created by the spark in the spark gap of the Marx generator caused many problems in the operation of highly sensitive electronic measuring devices. The use of the high speed image converter camera IMACON 600 was impossible due to the fact that the built-in time delay circuit in the camera was always triggered by the intense RF radiation from the Marx generator, even if the camera had been placed a large distance away from the laser system. Thus, time-resolved measurements on the expansion of the plasma could not be taken. It is therefore recommended that one build an effective shield against RF radiation around the CO_2 laser system, especially the Marx generator area.

It is further suggested to modify the charging circuit of the Marx generator inside the high-voltage panel in connection with a charge-trigger-dump switch. With this modification the Marx generator capacitors would be charged just prior to firing of the laser and the remaining amount of charge would be dumped after each shot, instead of the present construction where the full amount of charge was present at the Marx generator capcitors at all times during the daily operation.

Since the CO_2 laser system is sensitive to the surrounding conditions like air temperature and humidity, it is useful

to perform measurements of the same type on the same day to avoid errors in the data due to changes of atmospheric conditions.

It is recommended to use the high speed camera in the framing mode to obtain data on the expansion of a laser-produced spark in order to prove with time-resolved photographs the theoretical model of radiation-supported detonation- and blast waves. By placing electrostatic probes into the breakdown chamber data for the charge collection inside the plasma could be collected and the structure of the focused laser radiation could be studied in detail.

By applying a magnetic field its influence on the development of the laser spark could be investigated. In placing a solid target in the vicinity of the breakdown region, its interaction with the laser radiation could be examined together with the associated large recoil momentum. For studies of interaction of the laser radiation with solid targets it is suggested to try to optimize the resonant cavity of the laser and modify its operating conditions as was suggested by William F. Bassett [Ref. 34] in order to increase the output energy of the system up to 18 joules per pulse. Installation of a longer, antivibration optical bench as the mount for the system would minimize misalignment errors caused by vibrations.

APPENDIX A

CALCULATION OF WAVELENGTH BY THE HARTMANN DISPERSION FORMULA

In general the calculation of unknown wavelengths may be made either by linear interpolation between two nearby standard lines, or by use of a dispersion formula over a wide range [Ref. 35]. In the spectra obtained in this study many lines had to be determined. In this case linear interpolation is rather laborious and requires the identification of many standard lines. Furthermore, the accuracy depends nearly equally on the accuracy of the measurements of the two standard lines and on the accuracy of measurements of the unknown lines. The use of the Hartmann dispersion formula reduces the number of lines to be identified in advance to three lines, thus minimizing the effect of an error in the measurements of the standard lines. For wavelength calculations, the Hartmann dispersion formula can be written as

$$\lambda = \lambda_o + \frac{C}{d_o - d} , \tag{22}$$

where λ_o, C, and d_o are constants. For the determination of the three constants the comparator reading d of three lines of known wavelength is needed, in this case provided by the mercury-arc lamp. A form for the solution of the

three simultaneous equations, convenient for machine calculations, has been found by the University of Michigan. A numerical example, used with spectrum in air, is given below.

$\lambda_1 = 4358.33$ Å $\qquad d_1 = 0$

$\lambda_2 = 5460.73$ Å $\qquad d_2 = 113.3$ mm

$\lambda_3 = 5769.60$ Å $\qquad d_3 = 144.7$ mm

$\lambda_2 - \lambda_1 = 1102.4 \qquad d_2 - d_1 = 113.3$

$\lambda_3 - \lambda_1 = 1411.27 \qquad d_3 - d_1 = 144.7$

$d_3 - d_2 = 31.4$

$$\frac{d_2 - d_1}{\lambda_2 - \lambda_1} = 0.102775762 = a$$

$$\frac{d_3 - d_1}{\lambda_3 - \lambda_1} = 0.1025317622 = b$$

$$a - b = 0.0002439998$$

$$\frac{d_3 - d_2}{a - b} = 128689.052 = \frac{C}{d_o}$$

$$\lambda_o = \lambda_1 - \frac{C}{d_o} = -124330.722$$

$$d_o = a(\lambda_2 - \lambda_o) = 133339.41538$$

$$C = \frac{C}{d_o} \cdot d_o = 1716636719$$

$$(23) \qquad \lambda = \lambda_o + \frac{C}{d_o - d} = -124330.722 + \frac{1716636719}{133339.41538 - d}$$

It is desirable to check the solution by resubstitution calculating λ_1, λ_2, and λ_3 from d_1, d_2, and d_3. The λ_3-check in the example just given yields

$$\lambda_3 = -124330.722 + \frac{1716636719}{13339.41538 - 144.7}$$

$$= -124330.722 + 130100.322$$

$$= 5769.6$$

Checks of the other two wavelengths yielded the exact values used above.

The wavelengths for all unknown lines were determined by measuring their distance d with respect to the position of the line of reference wavelength λ_1 and inserting this value d into Equation (23). The obtained value for the unknown wavelength was compared to standard values for the respective background gas found in tables of spectral lines [Ref. 32], and the difference was never larger than 5 angstroms, yielding wavelength values of high accuracy.

Figure 1a

Gas Breakdown in Hydrogen at a Pressure of 6 atm.

Laser Peak Power:

1.35 megawatt

Focusing Lens:

Germanium,
f = 2.54 cm.

LASER ——→

Figure 1b

Gas Breakdown in Helium at a Pressure of 3 atm

Laser Peak Power:

2.65 megawatt

Focusing Lens:

Germanium
2.54 cm

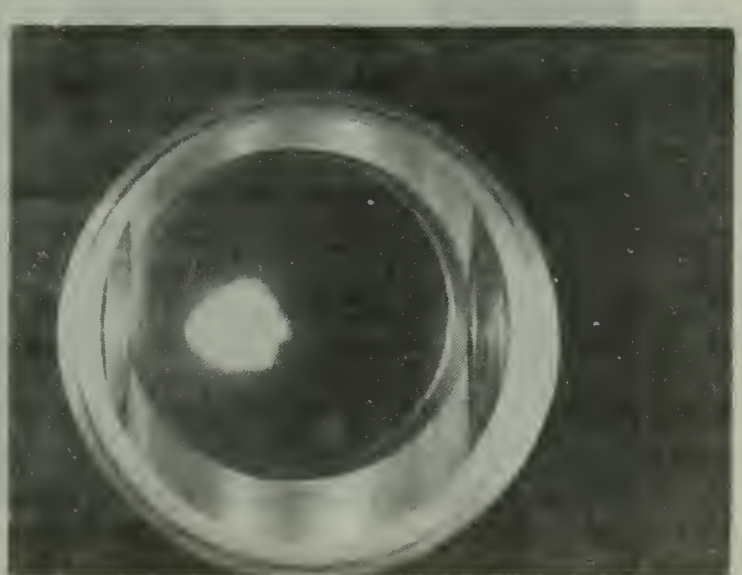

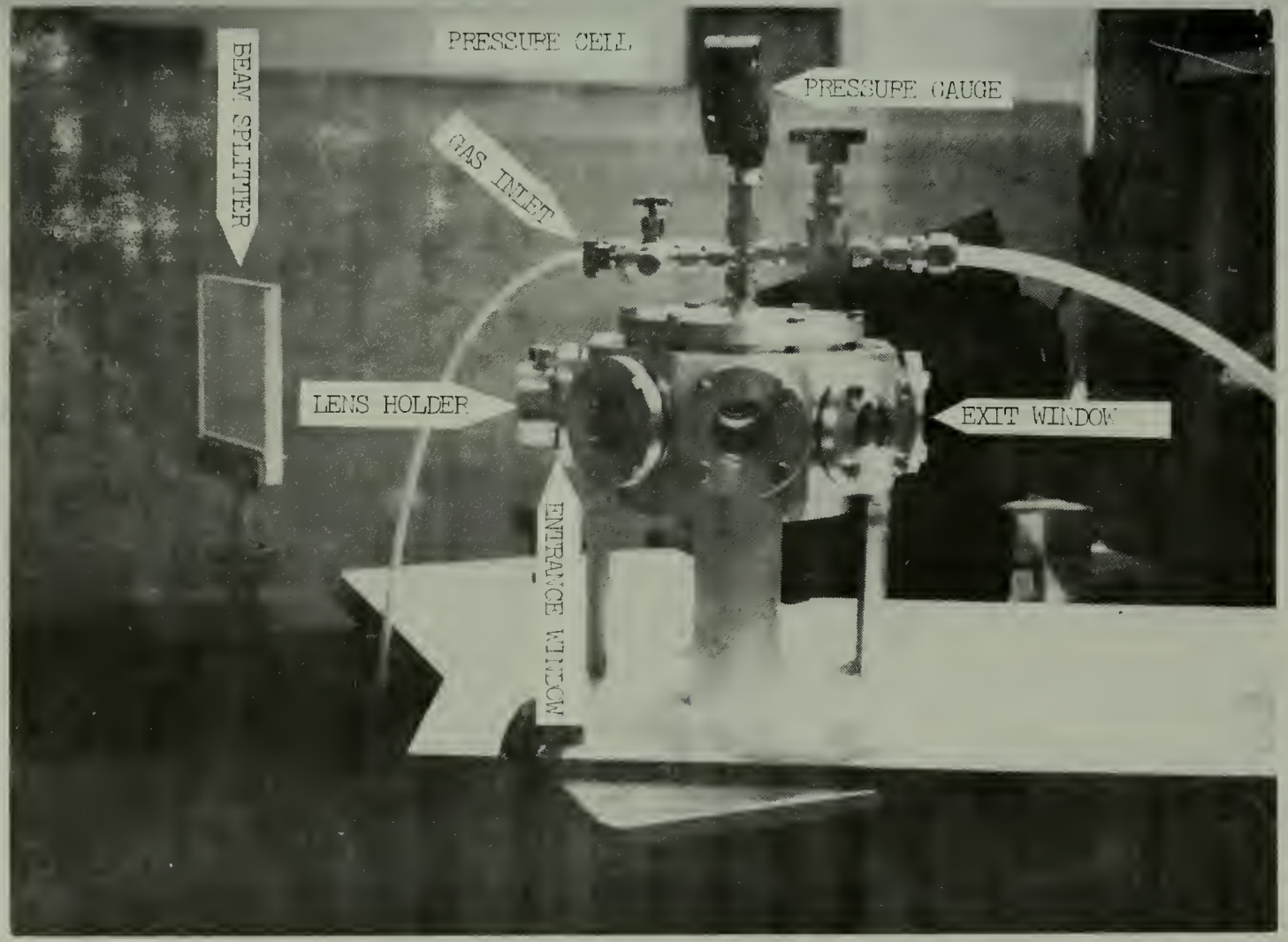
PRESSURE CELL
PRESSURE GAUGE
BEAM SPLITTER
GAS INLET
LENS HOLDER
EXIT WINDOW
ENTRANCE WINDOW

Figure 2

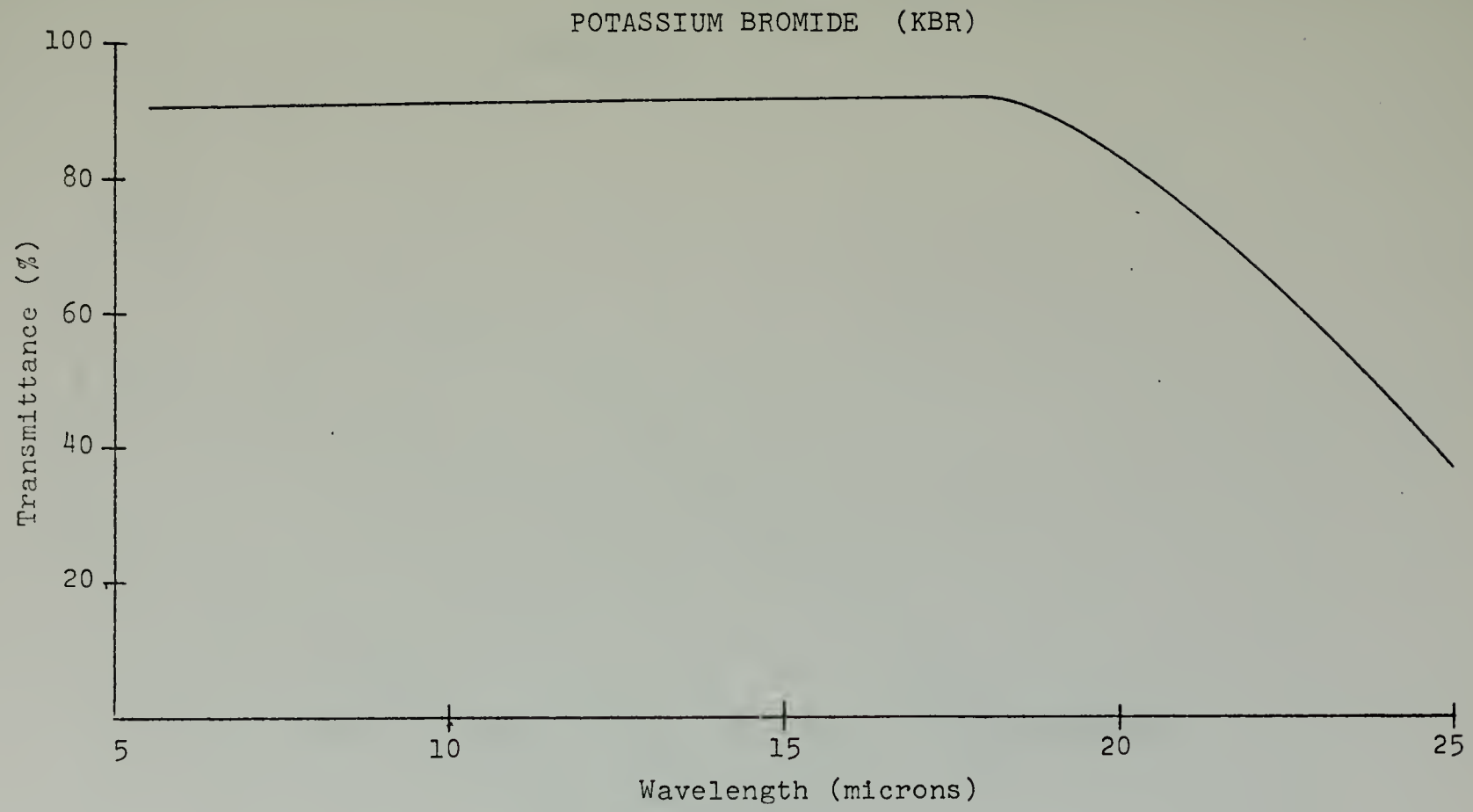
POTASSIUM BROMIDE (KBR)
100
80
60
40
20
Transmittance (%)
5
10
15
20
25
Wavelength (microns)

Figure 3

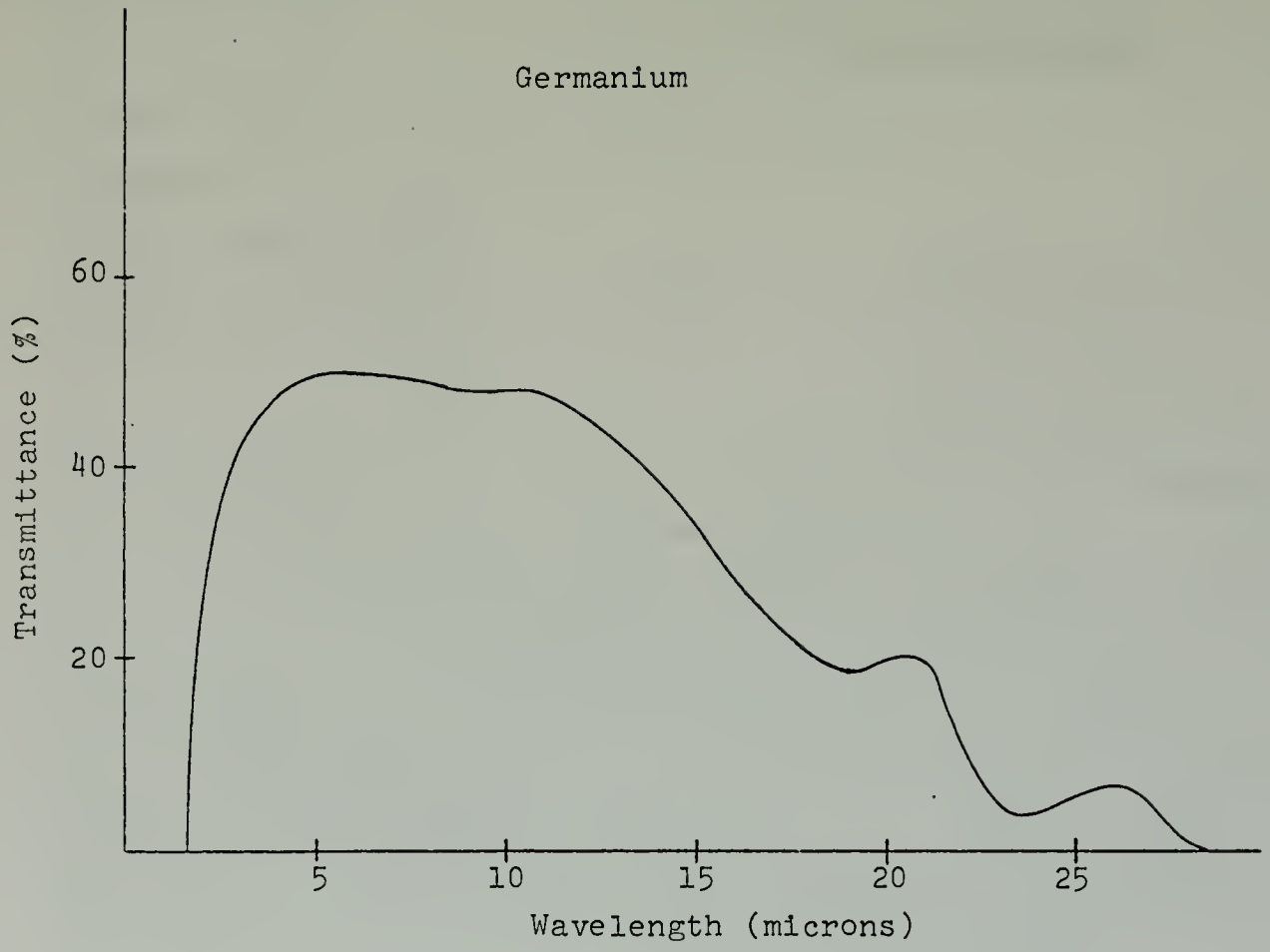
Germanium
Transmittance (%)
60
40
20
5
10
15
20
25
Wavelength (microns)

Figure 4

Experimental Setup

B Beamsplitter

A Aperture

D_1 Photondrag Detector

D_2 Detector UDT PIN 10

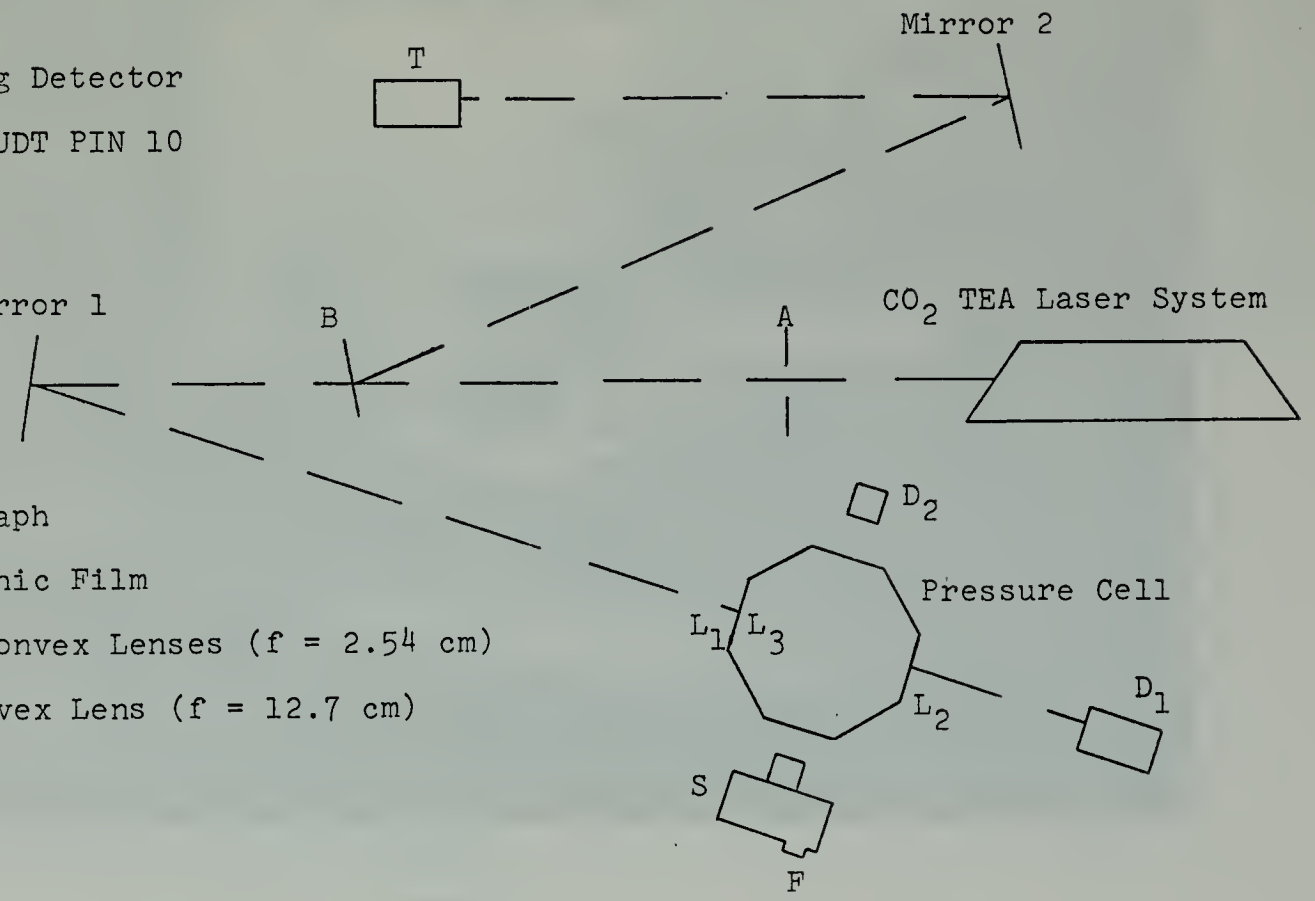

S Spectrograph

F Photographic Film

L_1 & L_2 Biconvex Lenses (f = 2.54 cm)

L_3 Planoconvex Lens (f = 12.7 cm)

Figure 5

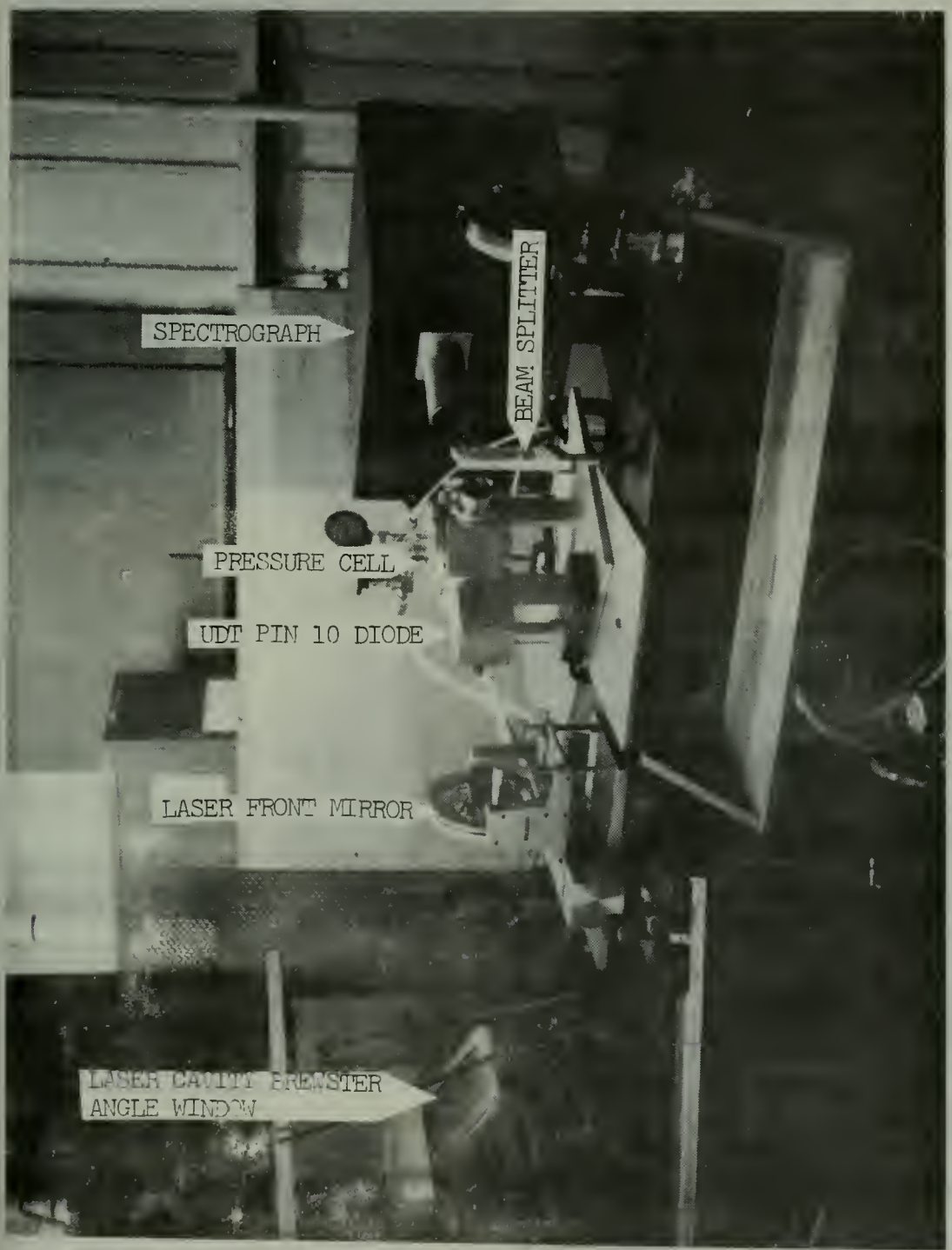
SPECTROGRAPH
BEAM SPLITTER
PRESSURE CELL
UDT PIN 10 DIODE
LASER FRONT MIRROR
LASER CAVITY BREWSTER
ANGLE WINDOW

Figure 6

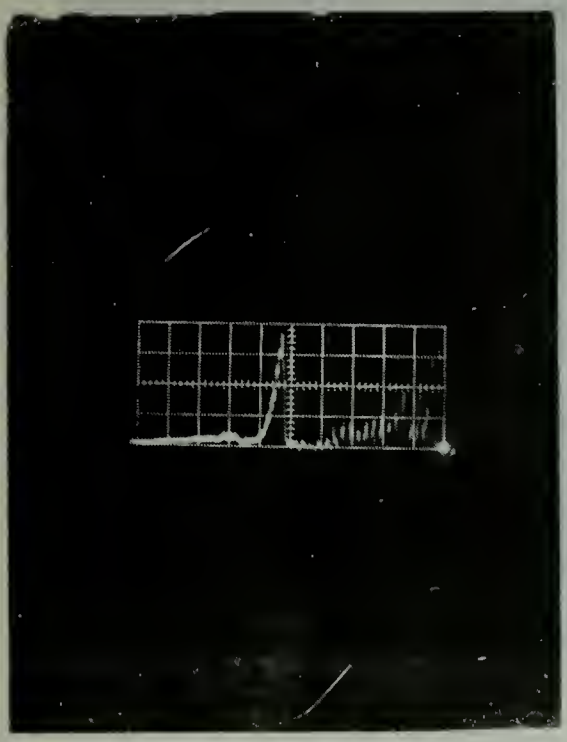

Figure 7a

Oscilloscope Trace of Forward Transmitted Laser Light without the Occurrence of Breakdown

Horizontal Scale:

0.5 microseconds/cm

Vertical Scale:

20 millivolt/cm

Gas: Nitrogen, 1 atm

Figure 7b

Oscilloscope Trace of Forward Transmitted Laser Light with the Occurrence of Breakdown

Horizontal Scale:

0.5 microseconds/cm

Vertical Scale:

20 millivolt/cm

Gas: Nitrogen, 1 atm

Figure 8a

Oscilloscope Trace of Forward Transmitted Laser Light Intensity taken by a photon drag detector

Horizontal Scale:

0.5 microseconds/cm

Vertical Scale:

20 millivolt/cm

Gas: Helium, 1 atm

Figure 8b

Oscilloscope Trace of 90° scattered visible Spark Light, taken with a UDT PIN 10 Photodiode

Horizontal Scale:

1 microsecond/cm

Vertical Scale:

0.1 volt/cm

Gas: Helium, 1 atm

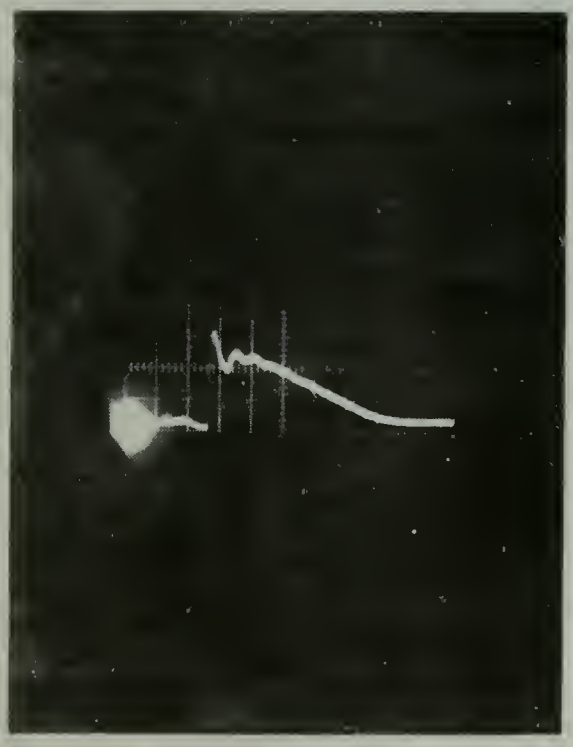

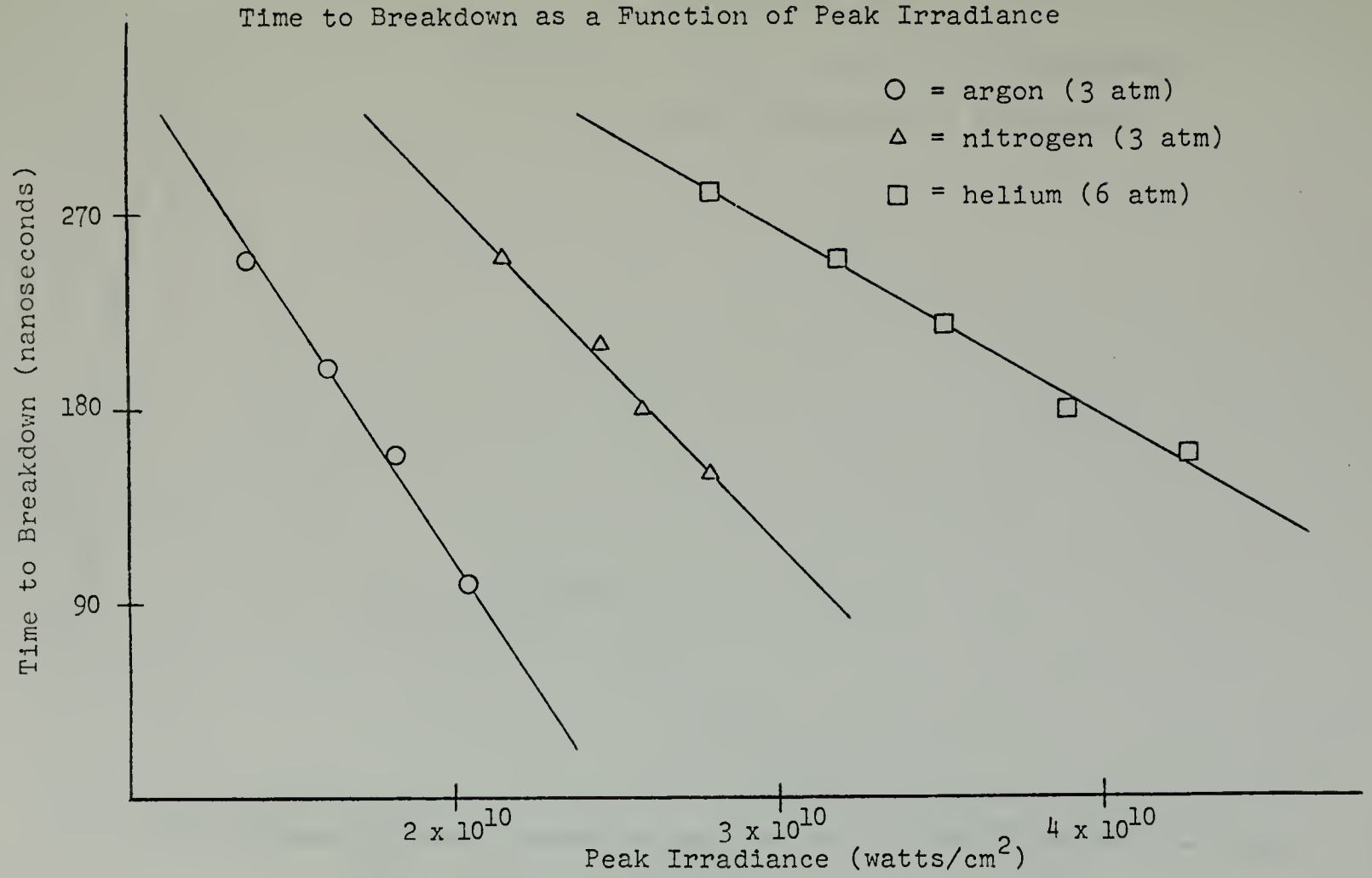
Time to Breakdown as a Function of Peak Irradiance
○ = argon (3 atm)
△ = nitrogen (3 atm)
□ = helium (6 atm)
Time to Breakdown (nanoseconds)
270
180
90
2 x 10^10
3 x 10^10
4 x 10^10
Peak Irradiance (watts/cm^2)

Figure 9

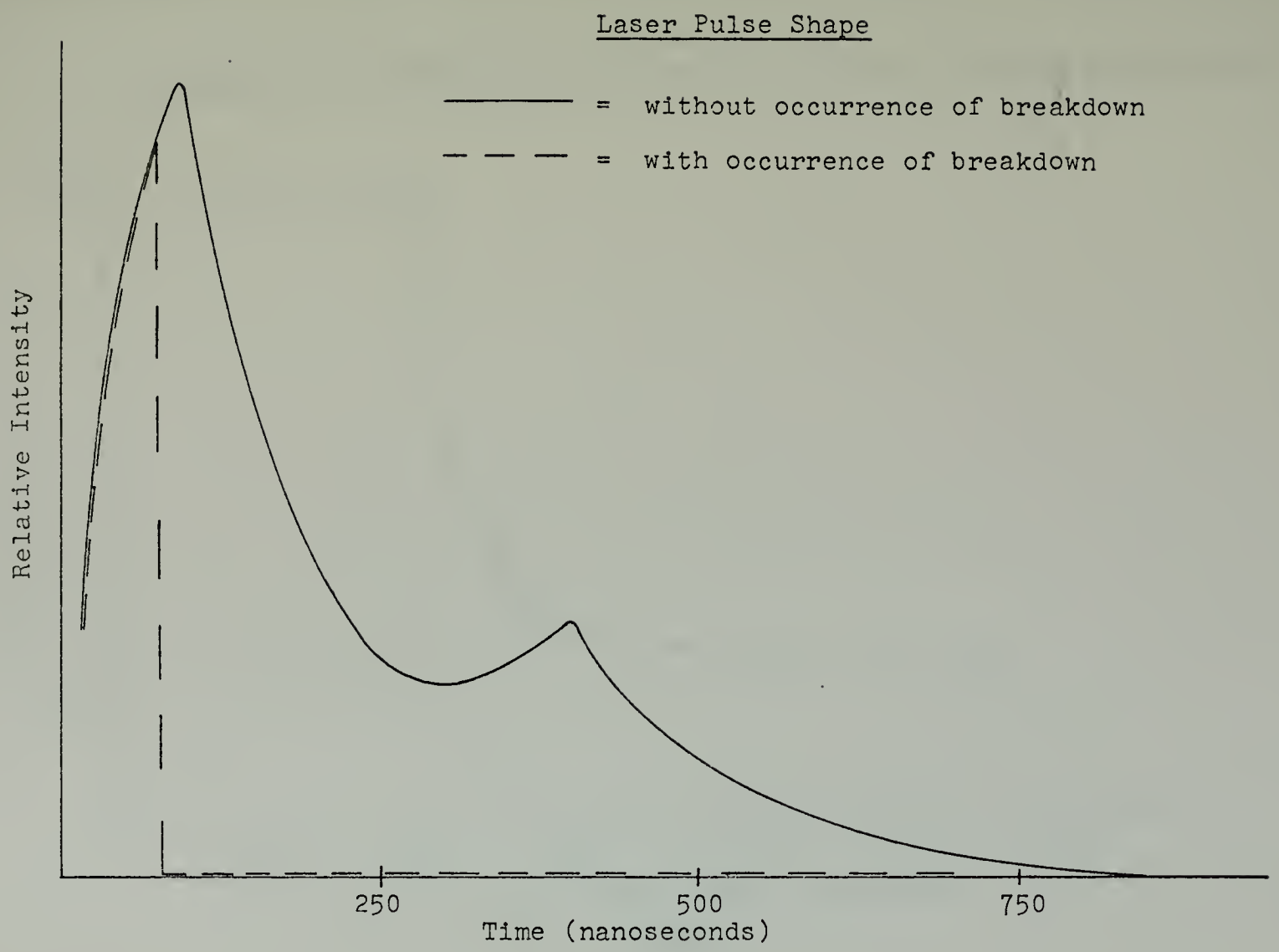
Laser Pulse Shape
= without occurrence of breakdown
= with occurrence of breakdown
Relative Intensity
250
500
750
Time (nanoseconds)

Figure 10

Transmission of Argon at a Pressure of 3 atm as a Function of Peak Power

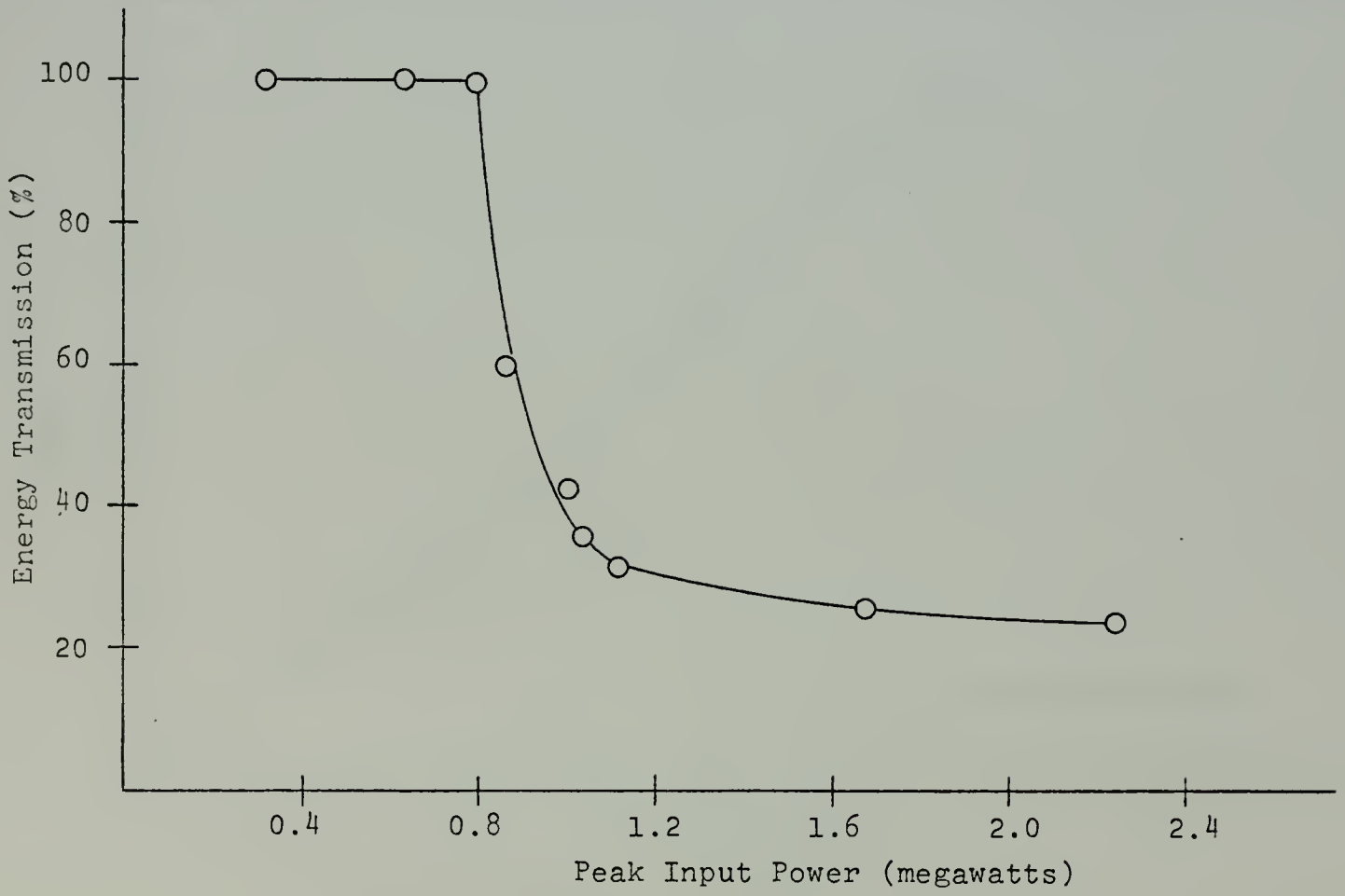

Figure 11

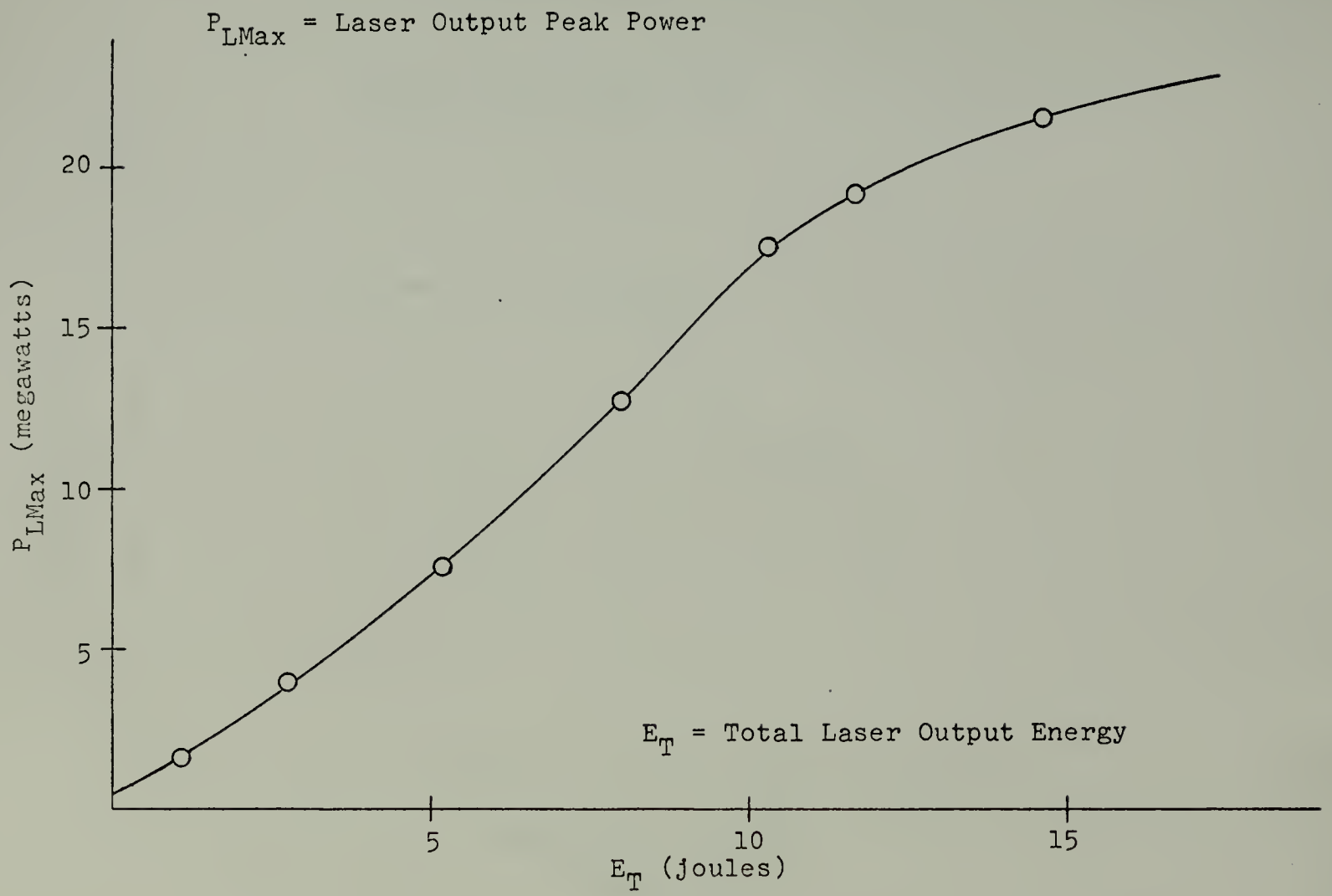
P_{LMax} = Laser Output Peak Power
20
15
10
5
P_{LMax} (megawatts)
E_T = Total Laser Output Energy
5
10
15
E_T (joules)

Figure 12

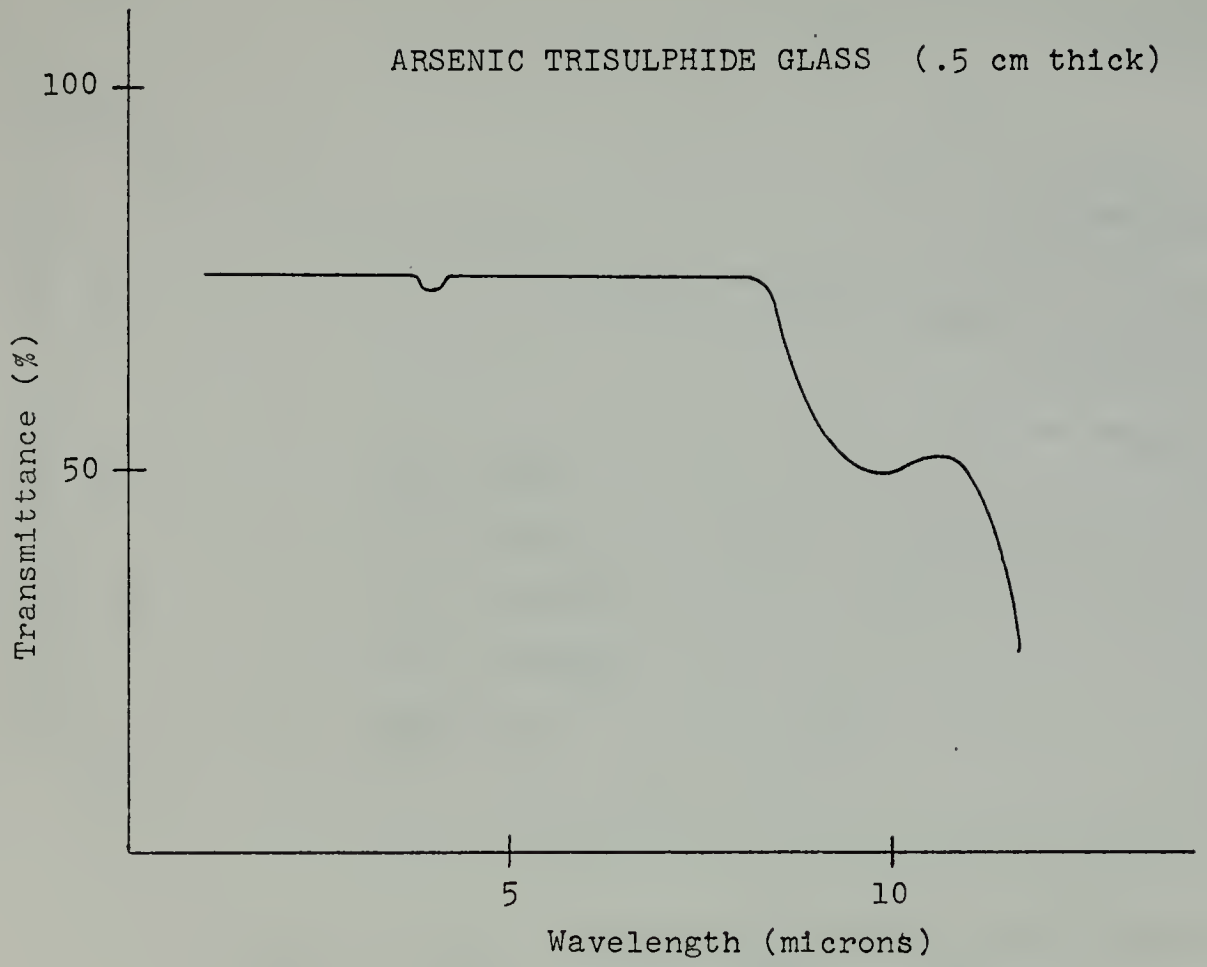
ARSENIC TRISULPHIDE GLASS (.5 cm thick)
100
50
Transmittance (%)
5
10
Wavelength (microns)

Figure 13

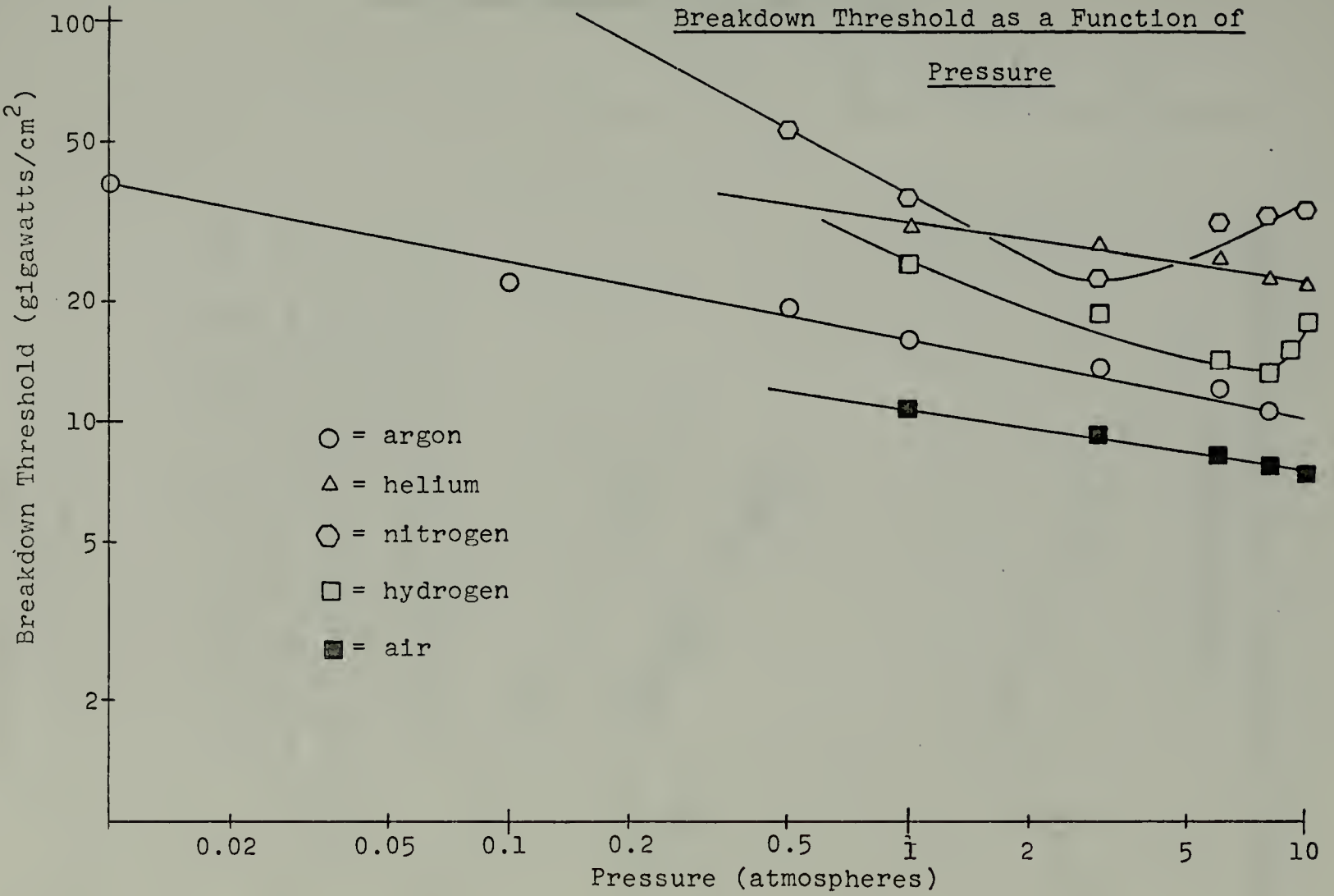
Breakdown Threshold as a Function of Pressure
Breakdown Threshold (gigawatts/cm^2)
100
50
20
10
5
2
○ = argon
△ = helium
⬡ = nitrogen
□ = hydrogen
■ = air
0.02
0.05
0.1
0.2
0.5
1
2
5
10
Pressure (atmospheres)

Figure 14

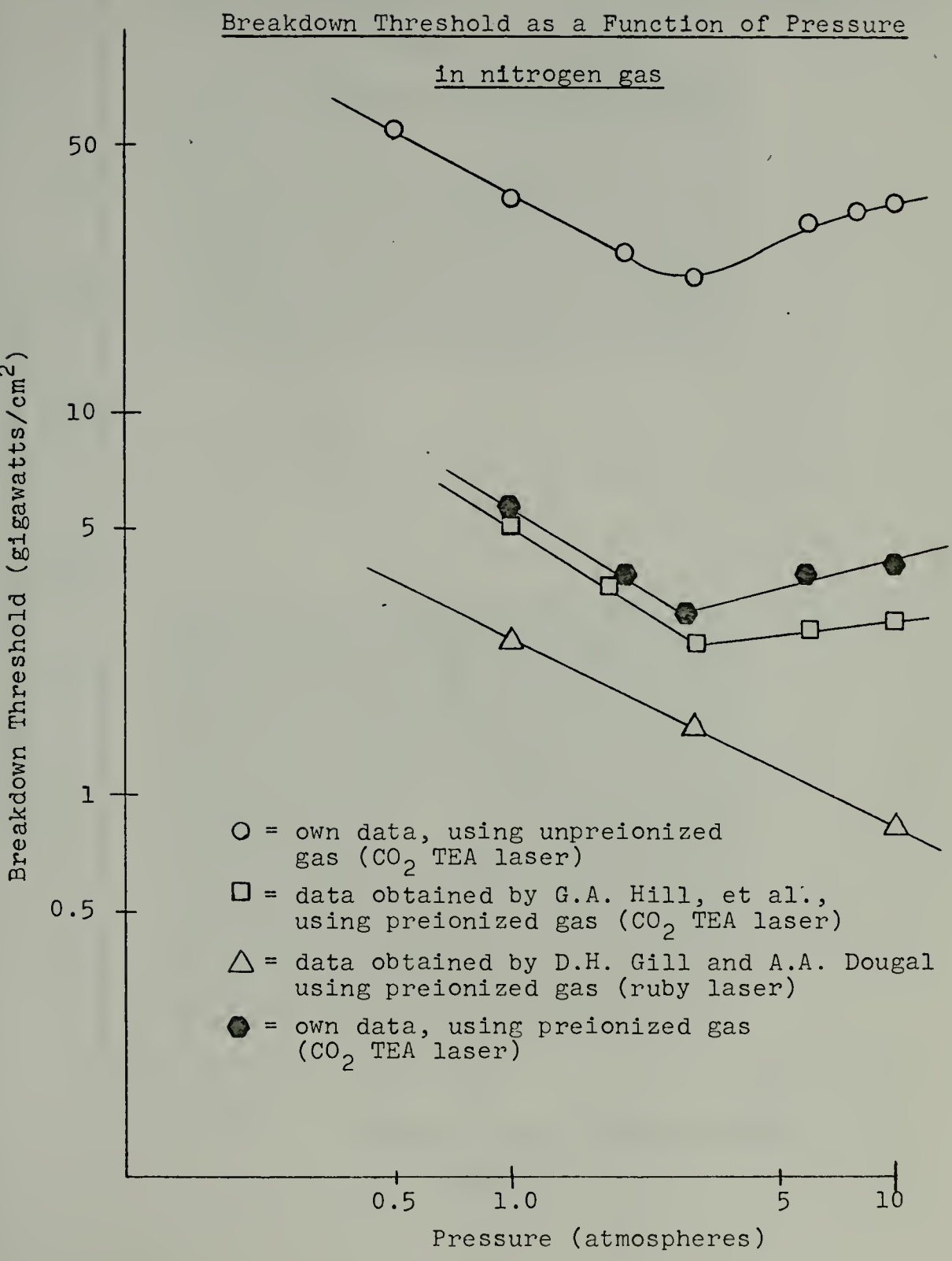
Breakdown Threshold as a Function of Pressure
in nitrogen gas
Breakdown Threshold (gigawatts/cm^2)
50
10
5
1
0.5
○ = own data, using unpreionized gas (CO_2 TEA laser)
□ = data obtained by G.A. Hill, et al., using preionized gas (CO_2 TEA laser)
△ = data obtained by D.H. Gill and A.A. Dougal using preionized gas (ruby laser)
⬢ = own data, using preionized gas (CO_2 TEA laser)
0.5
1.0
5
10
Pressure (atmospheres)

Figure 15

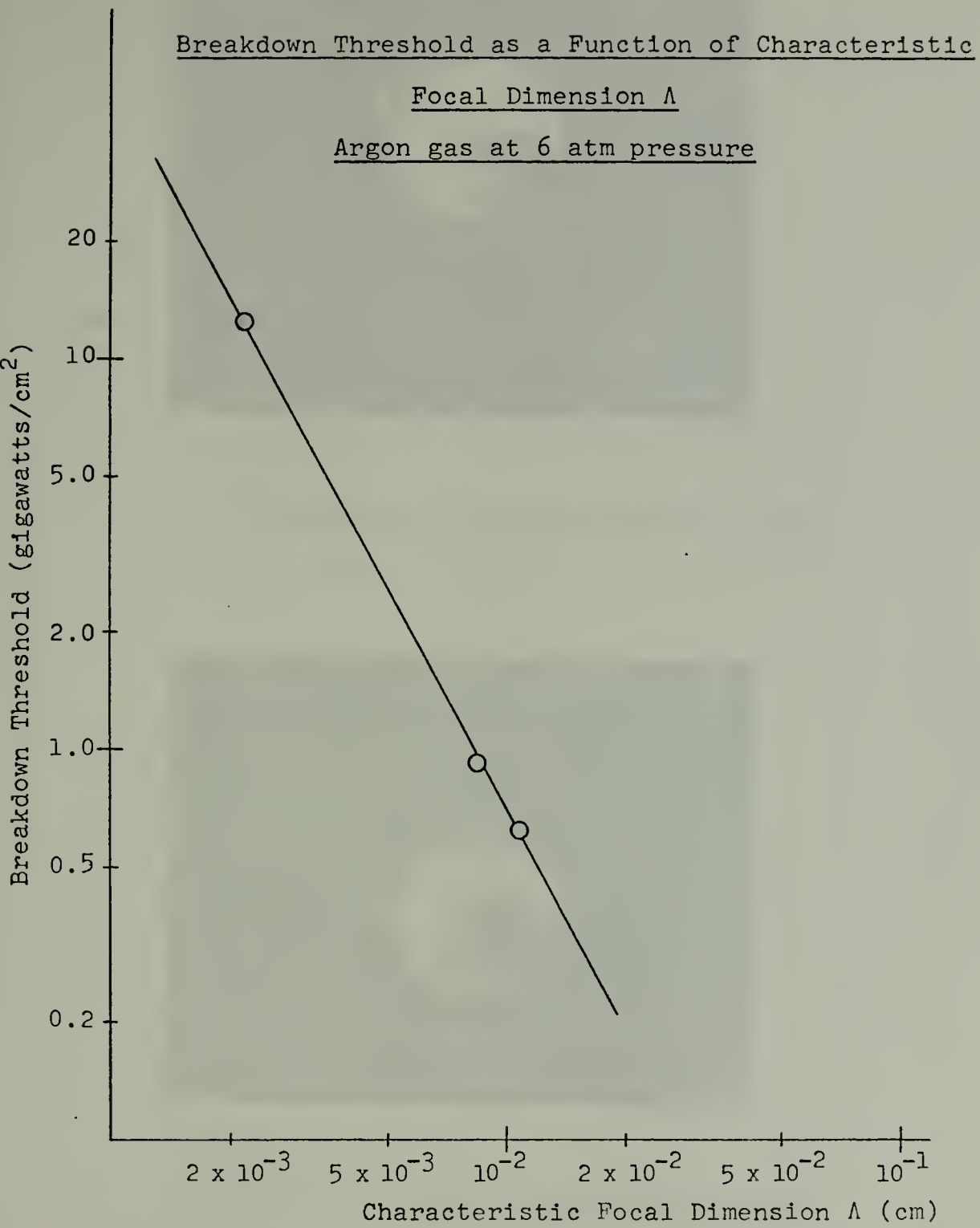
Breakdown Threshold as a Function of Characteristic
Focal Dimension Λ
Argon gas at 6 atm pressure
Breakdown Threshold (gigawatts/cm²)
20
10
5.0
2.0
1.0
0.5
0.2
2 x 10⁻³
5 x 10⁻³
10⁻²
2 x 10⁻²
5 x 10⁻²
10⁻¹
Characteristic Focal Dimension Λ (cm)

Figure 16

Figure 17a

Self-Focusing in Hydrogen Plasma at 6 atm

Self-Focusing Spots

Figure 17b

Self-Focusing in Hydrogen Plasma at 3 atm

In both pictures above, the laser beam was incident from the left.

Breakdown Threshold as a Function of Characteristic Focal Dimension Λ for Preionized Gases

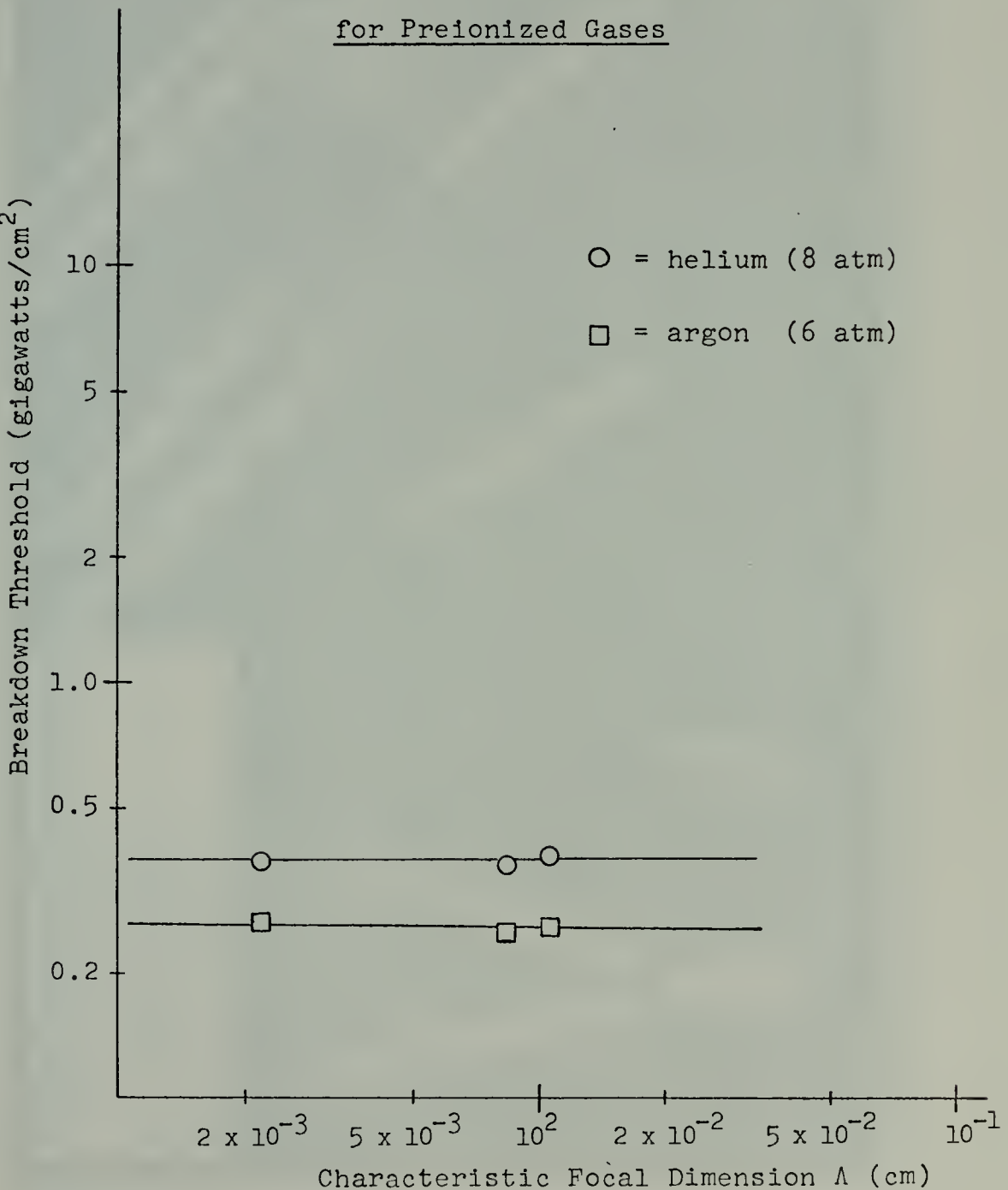

Figure 18

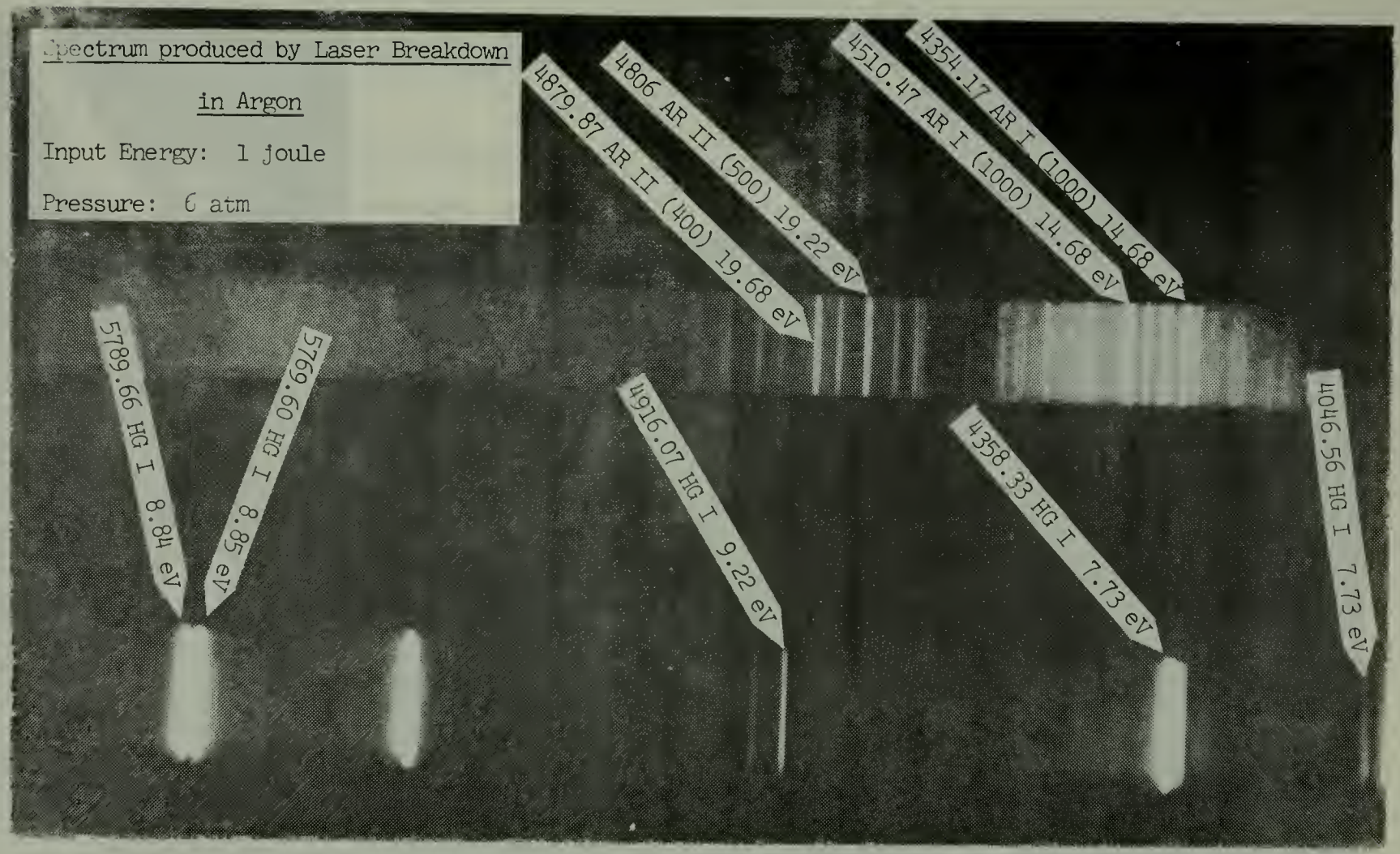
Spectrum produced by Laser Breakdown
in Argon
Input Energy: 1 joule
Pressure: 6 atm
4879.87 AR II (400) 19.68 eV
4806 AR II (500) 19.22 eV
4510.47 AR I (1000) 14.68 eV
4354.17 AR I (1000) 14.68 eV
5789.66 HG I 8.84 eV
5769.60 HG I 8.85 eV
4916.07 HG I 9.22 eV
4358.33 HG I 7.73 eV
4046.56 HG I 7.73 eV

Figure 19

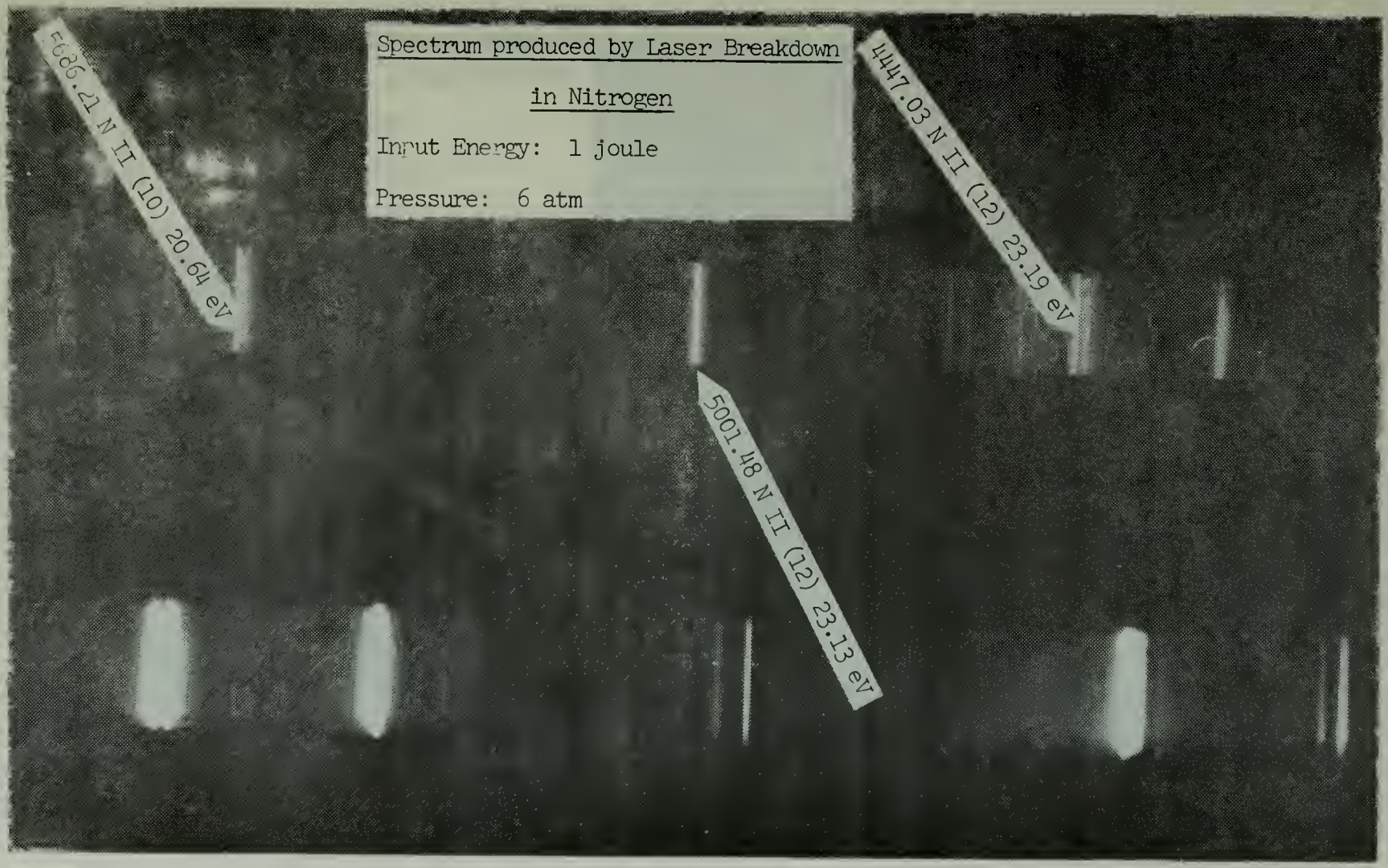
Spectrum produced by Laser Breakdown
in Nitrogen
Input Energy: 1 joule
Pressure: 6 atm
5005.17 N II (10) 20.64 eV
4447.03 N II (12) 23.19 eV
5001.48 N II (12) 23.13 eV

Figure 20

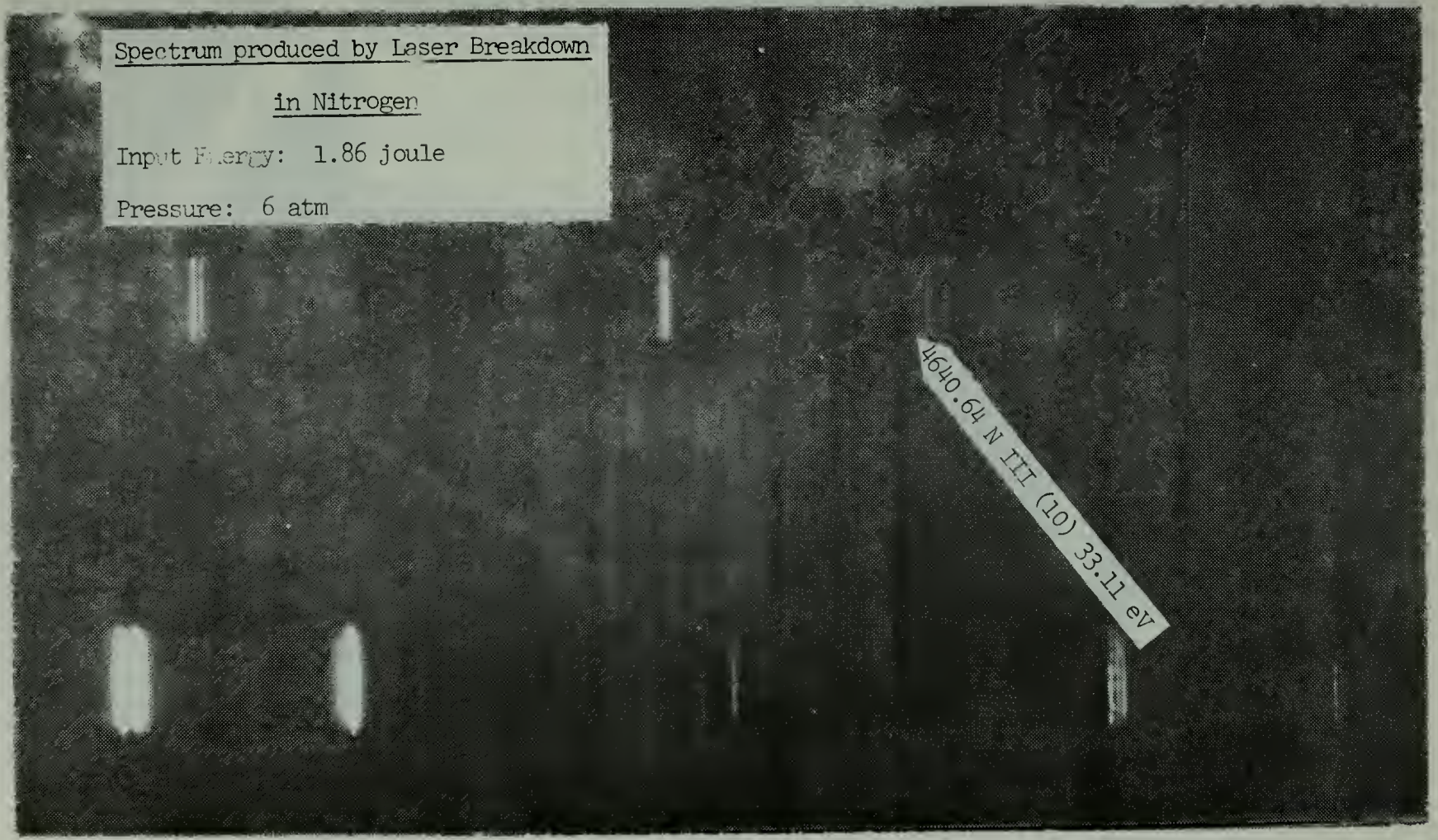
Spectrum produced by Laser Breakdown
in Nitrogen
Input Energy: 1.86 joule
Pressure: 6 atm
4640.64 N III (10) 33.11 eV

Figure 21

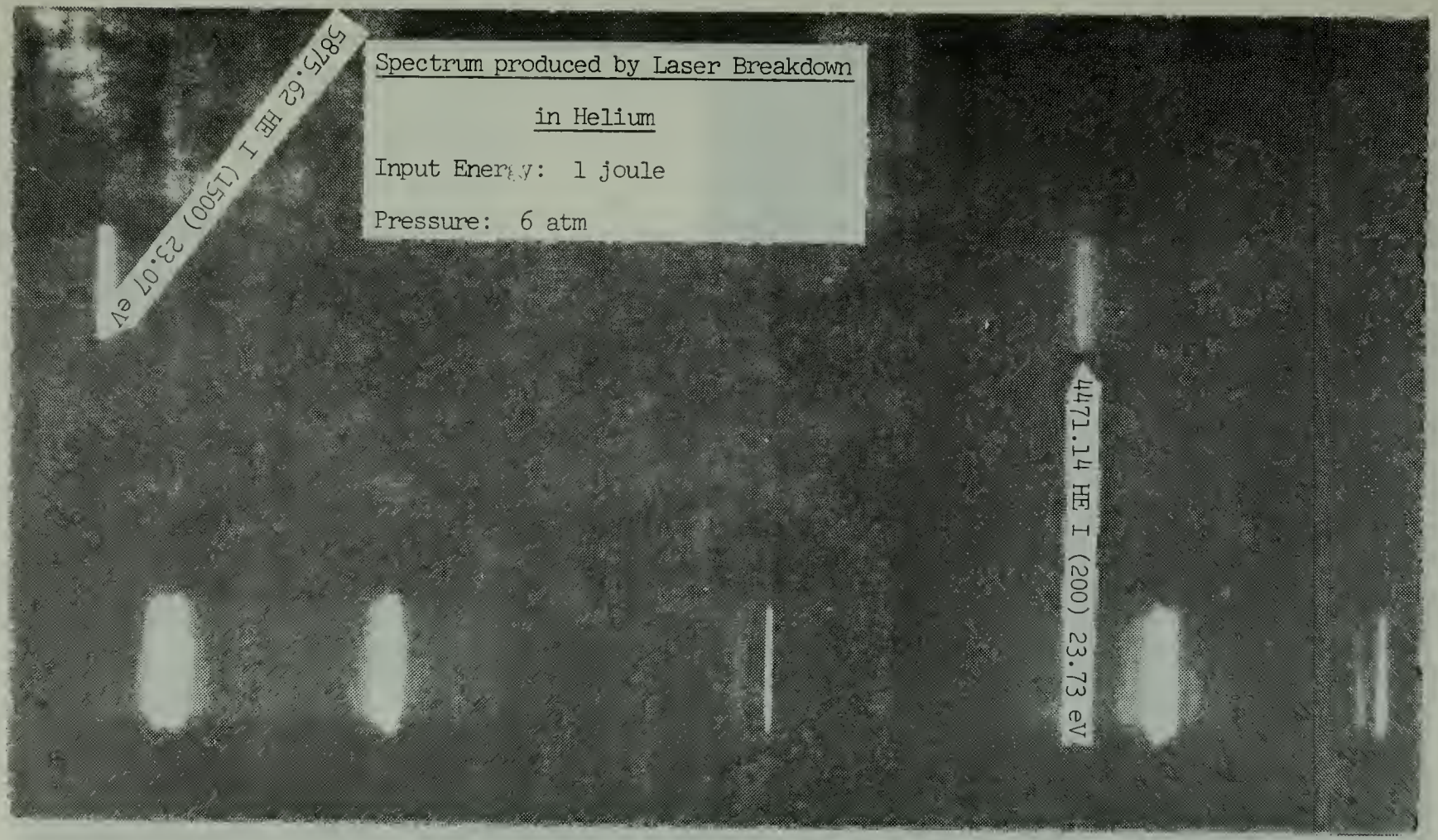
Spectrum produced by Laser Breakdown
in Helium
Input Energy: 1 joule
Pressure: 6 atm
5875.62 HE I (1500) 23.07 eV
4471.14 HE I (200) 23.73 eV

Figure 22

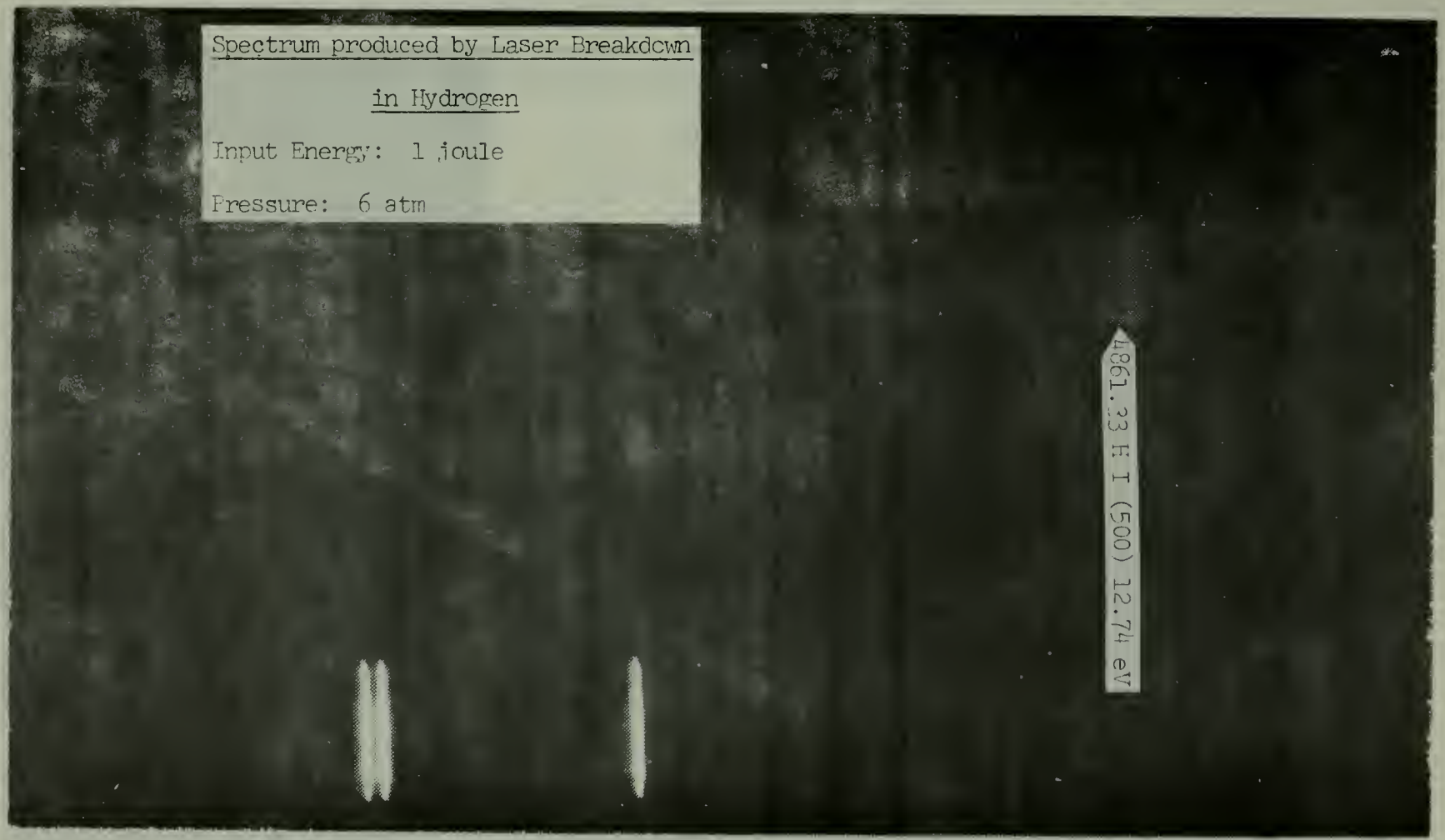
Spectrum produced by Laser Breakdown
in Hydrogen
Input Energy: 1 joule
Pressure: 6 atm
4861.33 H I (500) 12.74 eV

Figure 23

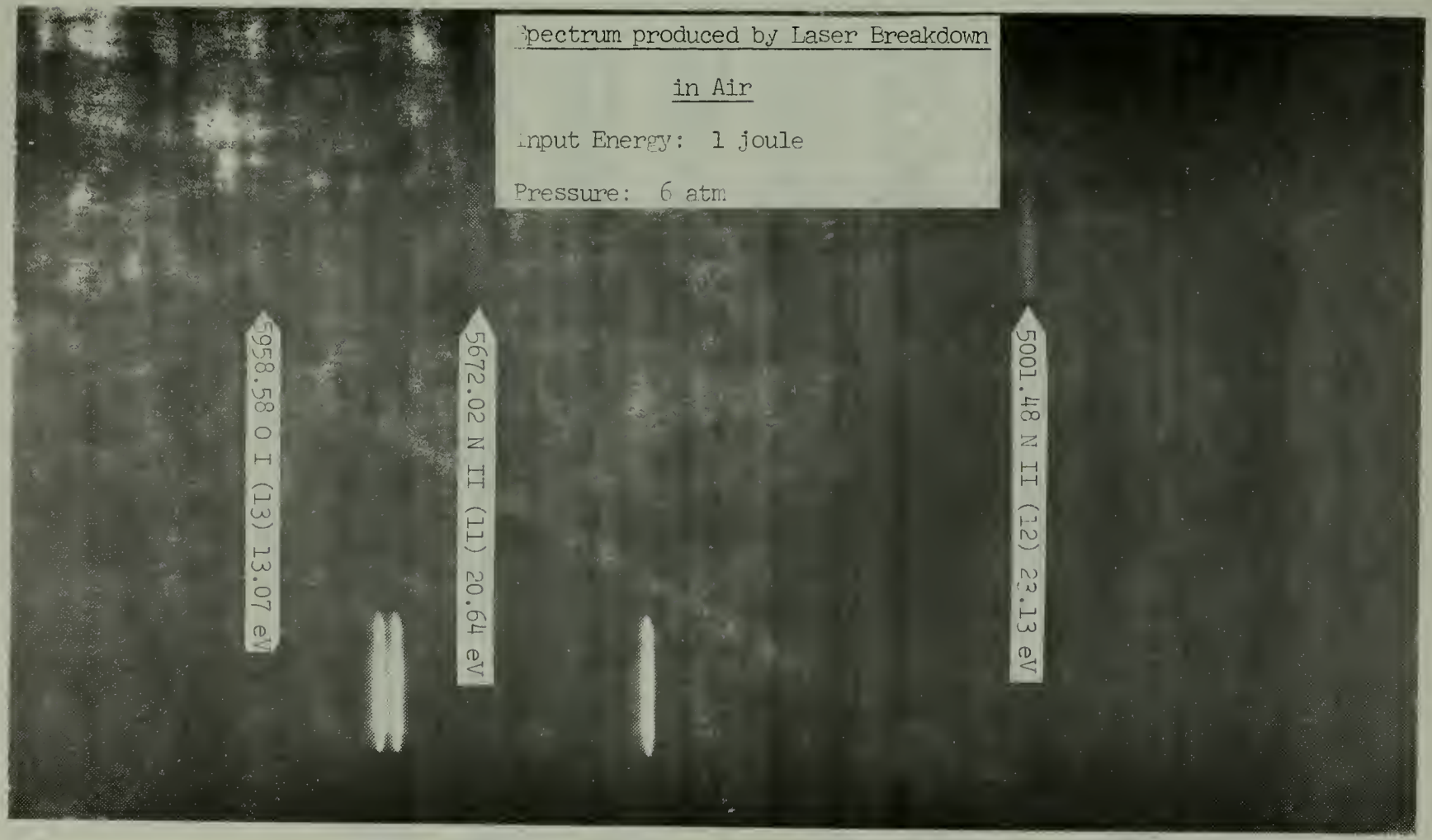
Spectrum produced by Laser Breakdown
in Air
Input Energy: 1 joule
Pressure: 6 atm
5958.58 O I (13) 13.07 eV
5672.02 N II (11) 20.64 eV
5001.48 N II (12) 23.13 eV

Figure 24

LIST OF REFERENCES

1. Lawrence Livermore Laboratory Report UCRL - 73931 Laser Possibilities in Pulsed Controlled Thermonuclear Fusion, by J. W. Shearer, p. 3, 24 August 1972.

2. Thomson, D. B., and Bailey, A. G., "Use of Theta-Pinches for Opacity Studies," Bulletin of the American Physical Society, v. 16, p. 1268, 17 November 1971.

3. Bebb, H. B., and Gold, A., "Multiphoton Ionization of Hydrogen and Rare-gas Atoms," Physical Review, v. 143, p. 1-24, 4 March 1966.

4. Tozer, B. A., "Theory of the Ionization of Gases by Laser Beams," Physical Review, v. 137, p. A1665-67, 15 March 1965.

5. Keldysh, L. V., "Ionization in the Field of a Strong Electromagnetic Wave," Soviet Physics, JETP, v. 20, p. 1307-14, May 1965.

6. Young, M., and Hercher, M., "Dynamics of Laser-induced Breakdown in Gases," Journal of Applied Physics, v. 38, p. 4393-4400, October 1967.

7. Browne, P. F., "Mechanism of Gas Breakdown by Lasers," Proceedings of the Physical Society of London, v. 86, p. 1323-31, December 1965.

8. Raizer, Y. P., "Breakdown and Heating of Gases Under the Influence of a Laser Beam," Soviet Physics, USPEKHI, v. 8, p. 650-73, March 1966.

9. Ramsden, S. A., and Savic, P., "A Radiative Detonation Model for the Development of a Laser-induced Spark in Air," Nature, v. 203, p. 1217-19, 19 September 1964.

10. Daiber, J. W., and Thompson, H. M., "Laser-driven Detonation Waves in Gases," Physics of Fluids, v. 10, p. 1162-69, June 1967.

11. Mandel'shtam, S. L., et al., "Investigation of the Spark Discharge Produced in Air by Focusing Laser Radiation," Soviet Physics, JETP, v. 22, p. 91-95, January 1966.

12. Panarella, E., and Savic, P., "Blast Waves from a Laser-induced Spark in Air," Canadian Journal of Physics, v. 46, p. 183-92, 1 February 1968.

13. Alcock, A. J., et al., "Expansion Mechanism in a Laser-produced Spark," Physical Review Letters, v. 20, p. 1095-97, 13 May 1968.

14. Griem, H. R., Plasma Spectroscopy, p. 445-52, McGraw-Hill, 1964.

15. Ramsden, S. A., and Davies, E. R., "Radiation Scattered from the Plasma Produced by a Focused Ruby Laser Beam," Physical Review Letters, v. 13, p. 227-29, 17 August 1964.

16. Dubois, D. F., et al., "Parametrically Excited Plasma Fluctuations," Laser Interaction and Related Plasma Phenomena, v. 2, Plenum Press, 1972.

17. Korobkin, V. V., and Alcock, A. J., "Self-focussing Effects Associated with Laser-induced Air Breakdown," Physical Review Letters, v. 21, p. 1433-35, 11 November 1968.

18. Rosenbaum, E. J., Physical Chemistry, p. 140, ACC, New York, 1970.

19. Offenberger, A. A., and Burnett, N. H., "CO_2 Laser-induced Gas Breakdown in Hydrogen," Journal of Applied Physics, v. 43, p. 4977-80, 12 December 1972.

20. Princeton University Report MATT-817, Anomalous Heating of Plasmas by Laser Irradiation, by P. Kaw, et al., p. 5, 17 December 1970.

21. Offenberger, A. A., et al., "Plasma Diagnostics Using CO_2 Laser Absorption and Interferometry," Journal of Applied Physics, v. 42, p. 574-77, February 1972.

22. Mandel'shtam, S. L., et al., "Study of the Spark Produced in Air by Focused Laser Radiation," Soviet Physics, JETP, v. 47, p. 2003-05, November 1964.

23. Oriel Optics Corporation, "Instruments and Components for Optical Research, 1971."

24. Private Communication with Nat Ceglio, Massachusetts Institute of Technology, Cambridge, Massachusetts, April 1974.

25. Smith, R. A., et al., The Detection and Measurement of Infra-red Radiation, p. 369, Clarendon Press, 1968.

26. Smith, D. C., "Gas Breakdown with 10.6 micrometer Wavelength CO_2 Laser Radiation," Journal of Applied Physics, v. 41, p. 4501-05, October 1970.

27. Minck, R. W., "Optical Frequency Electrical Discharge in Gases," Journal of Applied Physics, v. 35, p. 252-54, January 1964.

28. Hill, G. A. et al., "Breakdown Threshold in Rare and Molecular Gases Using Pulsed 10.6 micrometer Radiation," British Journal of Physics, Applied Physics, v. 5, p. L 97-99, 28 September 1972.

29. Korobkin, V. V., and Serov, R. V., "Investigation of Self-focussing of Neodymium Laser Radiation," Soviet Physics, JETP Letters, v. 6, p. 135-37, 1 September 1967.

30. MacDonald, A. D., Microwave Breakdown in Gases, p. 118, Wiley, 1966.

31. Smith, D. C., and Haught, A. F., "Energy-loss Processes in Optical-frequency Gas Breakdown," Physical Review Letters, v. 16, p. 1085-88, 13 June 1966.

32. Zaidel, A. N., et al., Tables of Spectral Lines, p. 499-507, IFI Plenum, 1970.

33. Daiber, J. W., and Winans, J. G., "Radiation from Laser-heated Plasmas in Nitrogen and Argon," Journal of the Optical Society of America, v. 58, p. 76-80, January 1968.

34. Bassett, W. F., Investigation and Operation of a Carbon Dioxide TEA Laser, M. S. Thesis, Naval Postgraduate School, Monterey, 1973.

35. Sawyer, R. A., Experimental Spectroscopy, p. 229-31, Prentice-Hall, 1948.

36. Gill, D. H., and Dougal, A. A., "Breakdown Minima due to Electron-Impact Ionization in Super-High-Pressure Gases Irradiated by a Focused Giant-Pulse Laser," Physical Review Letters, v. 15, p. 845, 29 November 1965.

37. Buscher, H. T., Tomlinson, R. G., and Damon, E. K., "Frequency Dependence of Optically Induced Gas Breakdown," Physical Review Letters, v. 15, p. 847, 29 November 1965.

INITIAL DISTRIBUTION LIST

		No. Copies
1.	Defense Documentation Center Cameron Station Alexandria, Virginia 22314	2
2.	DOKZENT Bundeswehr-See 53 Bonn Friedrich-Ebert-Allee 34 Fed. Rep. of Germany	1
3.	Marineamt -A1- 294 Wilhelmshaven Fed. Rep. of Germany	1
4.	Library, Code 0212 Naval Postgraduate School Monterey, California 93940	2
5.	Assoc. Professor Alf W. Cooper, Code 61Cr Department of Physics Naval Postgraduate School Monterey, California 93940	5
6.	Assoc. Professor Fred Schwirzke, Code 61Sw Deparment of Physics Naval Postgraduate School Monterey, California 93940	1
7.	Peter Behrens, LCDR FGN 3352 Einbeck Grimsehlstr. 41 Fed. Rep. of Germany	1
8.	Library Naval Postgraduate School Monterey, California 93940	2

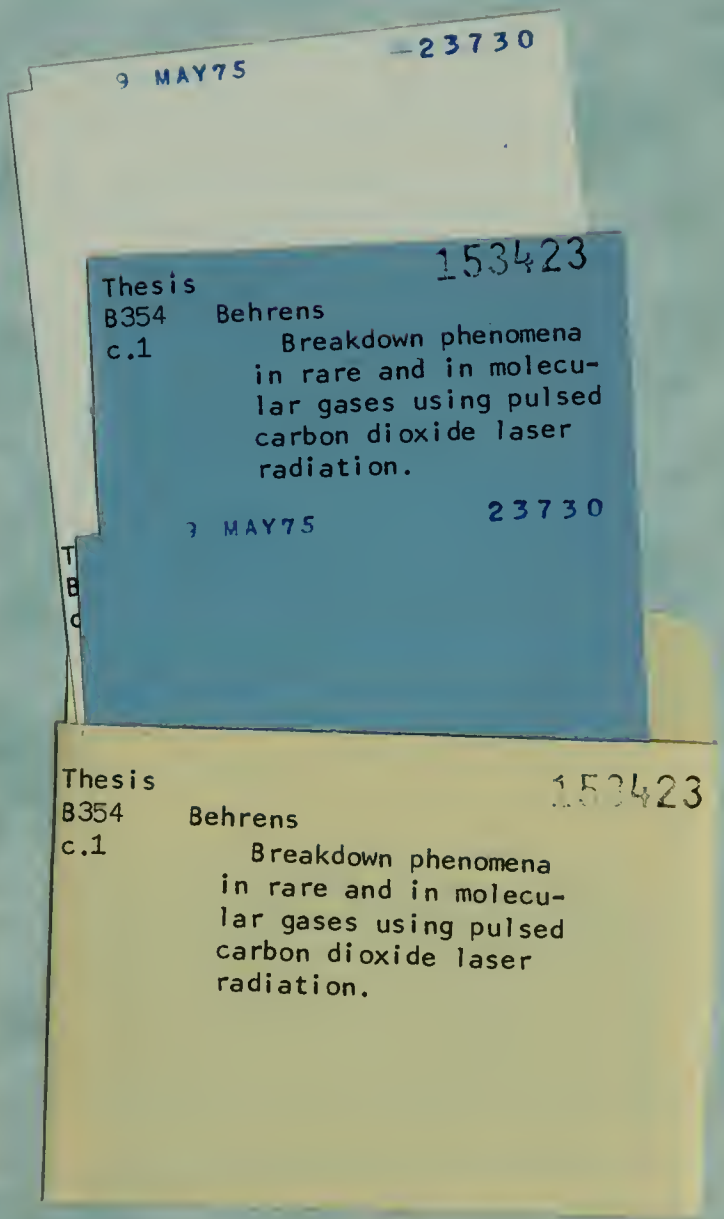
9 MAY75
23730
153423
Thesis
B354
c.1
Behrens
Breakdown phenomena in rare and in molecular gases using pulsed carbon dioxide laser radiation.
9 MAY75
23730
Thesis
B354
c.1
153423
Behrens
Breakdown phenomena in rare and in molecular gases using pulsed carbon dioxide laser radiation.